NASA TECHNICAL MEMORANDUM

THE EFFECT OF INITIAL FLOW NONUNIFORMITY
ON SECOND-STAGE FUEL INJECTION AND
COMBUSTION IN A SUPERSONIC DUCT

by Wm. Roger Russin

JUNE 1975

NATIONAL AERONAUTICS AND SPACE ADMINISTRATION
LANGLEY RESEARCH CENTER, HAMPTON, VIRGINIA 23665

1. Report No. NASA TM X-72667	2. Government Accession No.	3. Recipient's Catalog No.
4. Title and Subtitle THE EFFECT OF INITIAL FLOW NONUNIFORMITY ON SECOND-STAGE FUEL INJECTION AND COMBUSTION IN A SUPERSONIC DUCT		5. Report Date June 1975
		6. Performing Organization Code 37.430
7. Author(s) Wm. Roger Russin		8. Performing Organization Report No.
9. Performing Organization Name and Address NASA Langley Research Center Hampton, VA 23665		10. Work Unit No. 505-05-41-02
		11. Contract or Grant No.
12. Sponsoring Agency Name and Address National Aeronautics and Space Administration Washington, D.C. 20546		13. Type of Report and Period Covered Technical Memorandum
		14. Sponsoring Agency Code

15. Supplementary Notes

This is the final release of special information not suitable for formal publication which serves the following need: disseminates new information to those in industry and government agencies in referenceable form.

16. Abstract

The objective of this investigation was to evaluate the effects of flow nonuniformity on second-stage hydrogen fuel injection and combustion in supersonic flow. The first case, second-stage fuel injection into a uniform duct flow, produced data indicating that fuel mixing is considerably slower than estimates based on an empirical mixing cor: 'ation. The second-case, two-stage fuel injection (or second-stage fuel injection into a non-uniform duct flow), produced a large interaction between stages with extensive flow separation. For this case the measured wall pressure, heat transfer, and amount of reaction at the duct exit were significantly greater than estimates based on the mixing correlation. Substantially more second-stage fuel burned in the second case than in the first case. Overall effects of unmixedness/chemical kinetics were found not to be significant at the exit for stoichiometric fuel injection.

17. Key Words (Suggested by Author(s)) (STAR category underlined) Aircraft Propulsion and Power Supersonic combustion Fuel Injection	18. Distribution Statement Unclassified – Unlimited
19. Security Classif. (of this report) Unclassified	20. Security Classif. (of this page) Unclassified

21. No. of Pages 52	22. Price* $4.25

*Available from { The National Technical Information Service, Springfield, Virginia 22151

STIF/NASA Scientific and Technical Information Facility, P.O. Box 33, College Park, MD 20740

THE EFFECT OF INITIAL FLOW NONUNIFORMITY ON SECOND-STAGE
FUEL INJECTION AND COMBUSTION IN A SUPERSONIC DUCT

Wm. Roger Russin

Langley Research Center

SUMMARY

The objective of this investigation was to evaluate the effects of engine
flow nonuniformity on second-stage hydrogen fuel injection and combustion in
supersonic flow. The first case, second-stage fuel injection into a uniform
duct flow, produced data indicating that fuel mixing is considerably slower
than estimates based on an empirical mixing correlation. The second case, two-
stage fuel injection (or second-stage fuel injection into a nonuniform duct
flow), produced a large interaction between stages with extensive flow separa-
tion. For this case the measured wall pressure, heat transfer, and amount of
reaction at the duct exit were significantly greater than estimates based on
the mixing correlation. Substantially more second-stage fuel burned in the
second case than in the first case. Overall effects of unmixedness/chemical
kinetics were found not to be significant at the exit for stoichiometric fuel
injection.

INTRODUCTION

The concept of the supersonic combustion ramjet (scramjet) as a means of
airbreathing propulsion is attractive for flight at Mach numbers above 4. (See
refs. 1-4.) At these high speeds, portions of the vehicle external surface and
most of the engine surfaces would require active cooling. Hydrogen was selected
as a fuel for its high combustion heat release and as a regenerative coolant
for its high heat capacity. The basic goal of supersonic combustion research
is to reduce engine cooling requirements while still achieving high propulsive
efficiency. (See ref. 4.) The high propulsive efficiency is maintained when
the engine internal geometry is variable. However, for actively cooled flight
hardware the structural complexity attendant to variable geometry systems
generally results in the use of fixed or near fixed internal engine geometry.

One example of the latter engine geometry is the Hypersonic Research
Engine (HRE), which is an axisymmetric dual-mode scramjet engine. The HRE has
a translating inlet spike which allowed engine operation over the flight Mach
number range of 6 to 8 with full inlet air flow capture. Fuel injection was
essentially perpendicular to the engine air flow. At a flight Mach number of 8
all fuel was injected at the inlet throat, whereas at the lower Mach numbers

fuel was injected at the inlet throat and at various second-stage fuel injectors downstream. This staged fuel injection concept tailored the combustion heat release with the diverging combustor area downstream of the inlet throat to avoid thermal choking which would unstart the inlet air flow. This concept was evaluated in the component test program which provided the design information for the HRE. The effects of the engine flow nonuniformities caused by first-stage fuel injection were not understood.

The primary objective of this investigation was to evaluate the effects of engine flow nonuniformity on second-stage hydrogen fuel injection and combustion in supersonic flow. This was accomplished by using a two-dimensional combustion duct to simulate a geometric segment of the narrow annular combustor passage of the HRE. The first-stage fuel injector was in the constant area duct section and the second-stage fuel injector was downstream in the diverging duct section. Fuel injection in the combustion duct was sonic and perpendicular to the duct flow.

To achieve the test objective, two test conditions were defined. The first test condition (burner condition 1) produced a highly nonuniform profile at the the second-stage fuel injection location, while the second test condition (burner condition 2) produced a uniform profile. Both test conditions had the same mean flow properties at the second-stage injector location. The use of a combustion burner to provide the high temperature test gas to the combustion duct permitted a novel method of achieving the required test conditions. For burner condition 1, the oxygen content of the test gas was equal to that of air. With this test gas supplied to the duct, fuel was injected in two stages where the first-stage fuel was perpendicularly injected from top and bottom walls. The resulting combustion produced a nonuniform duct flow into which the bottom wall second-stage fuel was injected and burned. For burner condition 2, the combustion duct first-stage fuel was injected into the burner which increased the burner total temperature and reduced the burner oxygen content to simulate first-stage injection infinitely far upstream. The burner total pressure was then reduced to provide the same dynamic pressure as was calculated to have occurred in burner condition 1 at the second-stage injector location. This produced a uniform duct flow into which the bottom wall second-stage fuel was injected and burned.

Measurements include wall static pressure, wall heat transfer rate distributions, and overall duct wall heat transfer as well as pitot pressure and gas composition at the duct exit. These data are then compared with a one-dimensional theory which uses an empirical fuel mixing model (see ref. 4) derived from non-reactive fuel mixing data. (See ref. 5.)

SYMBOLS

A	combustor exit flow area (cm^2)
a, b	defined in ref. 5 (see eq. (1))
d	injector diameter, cm

dA	differential of combustor exit flow area (cm^2)
F	fraction of fuel reacted assuming measured η_c
F_c	fraction of fuel reacted assuming $\eta_c = 1.0$
f	integral unmixedness/kinetics factor
H_e	height of combustor duct at exit, cm
H_i	height of combustion duct at entrance, cm
p	wall static pressure, N/m^2
p_a	ambient pressure, N/m^2
p_f	fuel total pressure, N/m^2
p_h	burner total pressure, N/m^2
p_2	pitot pressure, N/m^2
q	heat transfer rate, $J/cm^2 sec$
q_r	fuel jet to duct flow dynamic pressure ratio
T_t	burner total temperature, K
W_h	burner test gas flow rate, Kg/sec
w	width of combustor duct, cm
X	nozzle contour axial coordinate, cm
x	distance downstream of combustor entrance, cm
$x_{\ell cm}$	length for complete mixing measured downstream of fuel injector, cm
y	lateral distance across flow at combustion duct exit, cm
Z	nozzle contour vertical coordinate, cm
z	vertical distance across flow at combustion duct exit, cm
α_{H_2}	mass fraction of combustion duct molecular hydrogen present in all forms
$\alpha_{H_2,r}$	mass fraction of combustion duct molecular hydrogen that has reacted assuming the measured η_c
$\alpha_{H_2,r,c}$	mass fraction of combustion duct molecular hydrogen that has reacted assuming $\eta_c = 1.0$

η_c	combustion efficiency
η_m	integral value of combustion duct fuel mixing efficiency
η_r	integral value of combustion duct fuel reaction efficiency
ϕ	equivalence ratio (= measured hydrogen to oxygen mass ratio divided by the same mass ratio for a stoichiometric mixture)
ϕ_r	reacted equivalence ratio

Superscripts:

$'$	prime defined in eq. (2)
$''$	double prime defined in eq. (3)

Subscripts:

ℓ	local (at point of measurement)
1	first fuel injector stage
2	second fuel injector stage

THEORY

One-Dimensional Flow Model

A detailed description of the theory applied in this research is reported in reference 6. The theory consists of a computer-programmed numerical solution of the integral form of the one-dimensional conservation equations assuming chemical equilibrium. The required input includes duct geometry, initial flow properties, fuel injection and fuel reaction rate distributions along the duct length, and fuel injection properties. Other input includes an average value for both the wall skin friction coefficient and wall surface temperature. The static pressure, static temperature, gas composition, and other duct flow properties are determined in a stepwise manner as a function of duct length. The momentum equation accounts for wall friction losses, and the energy equation accounts for heat transfer to the duct walls. For favorable pressure gradient regions, the heat transfer coefficient is determined from the skin friction coefficient using Reynolds' analogy. In adverse pressure gradient regions this heat transfer coefficient is increased by 50 percent, as is discussed in reference 6. The usefulness of the calculated results depends on the appropriateness of the input fuel reaction distribution.

4

Fuel Reaction Model

Since no perpendicular fuel injection mixing theories are available, the fuel reaction distribution of reference 4 was used. This distribution was derived from nonreactive, perpendicular, sonic injection mixing data presented in reference 5. This distribution, in tabular form, is given in table I. (See ref. 6.) This single-stage fuel schedule has been successfully applied in references 4 and 7 for perpendicular sonic fuel injection from combustion duct walls, and in reference 6 for perpendicular sonic fuel injection from a strut in a combustion duct.

TABLE I. – DIMENSIONLESS REACTION DISTRIBUTION FOR

SINGLE-STAGE PERPENDICULAR INJECTION

(Ref. 6)

ϕ_r/ϕ	$x/x_{\ell cm}$
0	0
0.19	0.01
0.75	0.20
0.85	0.40
0.94	0.70
1.00	1.00

The length for complete mixing for single-stage injection $x_{\ell cm}$ is calculated from

$$x_\ell = ad \, (q_r)^b \tag{1}$$

where d is the injector diameter, and a and b are parameters from the correlations of reference 5 that depend on injector spacing.

Construction of the fuel reaction distribution for two-stage fuel injection is based on the single-stage distribution given in table I and the flow physics as discussed below. As shown in reference 5, if the distance between the stages is on the order of the first-stage length for complete mixing, then the second-stage fuel is injected into a duct flow having nonuniform velocity and concentration profiles across the flow resulting from first-stage fuel mixing and combustion.

To account for the effect of uniform depletion of the main duct flow oxygen by first-stage combustion, equation A(9) in reference 8 was used.

$$(\phi_r/\phi_2)' = (1 - \phi_1) \frac{\phi_r}{\phi_2} \qquad (2)$$

However, use of this equation predicts thermal choking of the combustion duct which is contrary to observation. Since the very rapid initial burning indicated by the distribution of table I probably does not occur when injecting into a highly nonuniform stream, this part of the distribution was eliminated and the remainder of the distribution was re-normalized using equation 3.

$$(\phi_r/\phi_2)'' = \frac{(\phi_r/\phi)' - 0.19 \, (1 - \phi_1)}{1.0 - 0.19} \qquad (3)$$

The length for complete mixing of the second-stage fuel is also computed using equation (1), and the resulting $\phi_2(\phi_r/\phi_2)''$ distribution is then added to the first-stage $\phi_1(\phi_r/\phi_1)$ distribution by superposition, as shown in sketch (a).
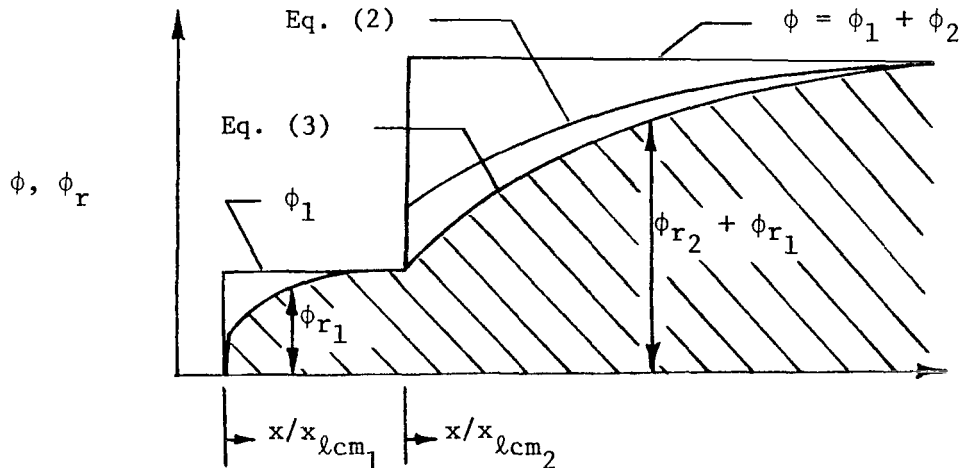
sketch (a)

It should be noted that equation (3) is used for theoretical predictions in this report, but remains an unverified approximation.

APPARATUS AND PROCEDURE

Combustion Burner and Nozzle

The hydrogen-oxygen-air burner shown in figure 1 supplied the test gas for the experiments. This low velocity burner was supplied with high-pressure gases in proportions to achieve the desired burner conditions. Details of the burner, its operation, and performance are contained in reference 9. For burner condition 1, the burner is controlled to supply oxygen-replenished test gas containing approximately 21 percent oxygen, 55 percent nitrogen, and 24 percent water vapor by volume with a stagnation temperature and pressure of about 1680 K and 2.2 MN/m^2, respectively. For burner condition 2, the corresponding numbers are approximately 16 percent oxygen, 52 percent nitrogen, and 32 percent water vapor by volume with a stagnation temperature and pressure of 2100 K and 2.1 MN/m^2, respectively. Figure 2 shows the contoured two-dimensional converging-diverging nozzle which expands the test gas to a nominal exit Mach number of 2.75. According to reference 10, burner nozzle exit surveys indicate a nearly constant stagnation temperature with variation in the local values of less than ± 75 K.

Combustion Duct

The two-dimensional combustion duct used in this investigation is shown in figure 1 directly connected and sealed to the nozzle exit plane. Referring to the schematic in figure 3 and the photograph of the top and bottom walls in figure 4, the duct is a constant 17.0 cm wide, and 3.86 cm high at the entrance area section for the first 20.7 cm. The constant area section is followed by a diverging section having an overall area ratio of approximately 1.5. The first-stage injector blocks are located directly opposite each other near the mid-point of the constant area section. Circular injector orifices are 0.18 cm diameter at an equal spacing of 2.79 cm. The orifice injection angles are perpendicular to the surface. The first-stage injectors in top and bottom blocks are interdigitated with those of the opposing block with six injector orifices on the top and five on the bottom. The second-stage injector block is located on the bottom wall just downstream of the start of the diverging duct section. These injection orifices are 0.38 cm diameter, have the same physical spacing as the first-stage, and are interdigitated with those of the first-stage injectors on the bottom wall. Ambient temperature hydrogen is supplied to the injectors which operate choked with a nominal discharge coefficient of 0.80.

Instrumentation

The primary sources of data are: (1) a row of static pressure ports along the centerline of the top and bottom walls of the combustion duct connected to four scanivalves, (2) water cooling temperature rises and flow rates through several individual blocks in the duct's bottom wall, and (3) pitot pressure and gas sample surveys at the duct exit. Additional measurements include the burner stagnation pressure, flow rates of the supply gases, and the duct cooling water

flow rate and temperature rise. The latter allows calculation of the overall heat flux to the duct walls. The local heat transfer rates on the bottom wall were calculated from measurements of the water flow rates and temperature rises through both knuckle joints, both fuel injector blocks, and the three blank blocks in the diverging duct section. (See figures 3 and 4.) The knuckle joints spanned the entire duct width. The fuel injector blocks and three blank blocks spanned 92 percent of the duct width. The knuckle joints and fuel injector blocks were connected in series in one circuit and the blank blocks in series in another circuit having water cooling flow rates of 0.18 and 0.33 kg/sec, respectively.

Survey Rake

The instream measurements of pitot pressure and gas composition were acquired using the nine-probe rake shown in figures 5(a) and 5(b). This probe rake was traversed vertically across the flow 0.3 cm downstream of the duct exit stopping at discrete points to acquire data. During a test run the option was to acquire pitot pressure at five vertical locations, or a pitot pressure and a gas sample at one vertical location. The pitot pressure transducer outputs were recorded on FM tape. The water-cooled rake exhausted water from the probe tip base, as shown in figure 5(b). The coordinate system used in presenting the data is given in figure 5(c).

Gas Sample Collection System

Each pitot probe in figure 5 is connected to a 75 cc sample collection bottle which in turn is connected to a vacuum reservoir. Remotely controlled valves on the upstream and downstream end of the bottle allow the operator to collect the sample as follows: (1) the probe is inserted to a position in the duct flow with the valves closed, (2) pitot pressure is recorded for one second, (3) both valves are opened for three seconds to allow a representative sample of the gas to move through the bottle, (4) the downstream valve was closed and the bottle allowed to fill for three seconds, and (5) the upstream valve was closed securing the sample. This sample is at approximately 40 percent of the pitot pressure. Since the tubing is unheated, water condenses in the lines, and hence no meaningful quantity of water is expected in the sample bottle. The bottles are then removed from the test area and gas composition determined. The ability to determine the combustion efficiency depends directly on the quenching ability of the probe as is discussed in reference 10.

Gas Sample Analysis

A standard gas chromatograph was used to measure the volume fractions of the helium, hydrogen, oxygen, nitrogen, and argon. These volume fractions are determined on a dry basis since no measure of water was obtained. In order to calculate the water content, helium is used as the tracer of the oxygen supplied and nitrogen is used as the tracer of the oxygen from the air supplied to the

8

burner. The tracer element is assumed to remain in a fixed proportion to the supply gas in which it was originally contained. With these tracers, the mass fraction of molecular oxygen in all forms can be calculated. The difference between the calculated and the measured oxygen mass fractions is due to the formation of water by reaction with hydrogen. With this difference the mass fraction of water can be calculated and the volume fractions on the dry basis are then converted to the wet basis. The measured hydrogen plus the calculated water mass fractions represent hydrogen from both the burner and combustion duct. Since the burner provides a nearly uniform mixture as previously discussed, the burner hydrogen can then be calculated using nitrogen as a tracer for the burner test gas. In each sample bottle, the difference between the measured total mass fraction of hydrogen in all forms and the calculated burner hydrogen, is attributed to the hydrogen injected in the combsution duct. With these results, the local equivalence ratio and combustion efficiency as well as the total and reacted local mass fractions of combustion duct hydrogen, can be calculated.

Measurement Accuracy

The strain gage transducer measurements of the wall pressures in the form of p/p_h are repeatable within ± 0.003. Due to variation in test conditions with time, another source of possible error could be the fact that six seconds were required for the scanivalves to sequence and acquire the wall pressure data. The pressures were allowed to settle for 0.13 seconds and the analog transducer signal was integrated over 16.6 milliseconds and digitally recorded. The error here in p/p_h is near ± 0.003 as determined from comparing repeated tests.

Local heat transfer measurement is estimated to have a repeatability within ± 20 percent. This is mainly due to the small temperature differences measured across the various inserted blocks where the repeatability of the temperature measurement is within ± 0.5 K.

Gas composition measurement was found to be repeatable within ± 0.01 by volume fraction as is disucssed in reference 10. Typically mass-weighted integrations of the duct exit flow composition, as compared to the measured supply gas flow rates, could be 10 to 20 percent in error. Lack of static pressure measurements across the exit flow precluded that check on the overall accuracy of the composition data in this report.

Test Procedure

The first step in the procedure was to establish the desired burner conditions. Performance plots necessary to determine the relative flow rates of the supply gases to the burner for the desired test conditions are given in reference 9. The next step was to establish the fuel conditions in the combustion duct and insert the probe at the duct exit. A computer-controlled data acquisition system sequences the scanivalves, and records digitally on magnetic tape these pressure transducer signals and other measurements related to the burner and combustion duct operation. Immediately after the test, the computer provides

a limited printout of reduced data indicating the burner and combustion duct fuel conditions achieved.

RESULTS AND DISCUSSION

The tests conducted to achieve the objective stated in the Introduction of this report are summarized in table 2. Total temperature, T_t, in the burner was determined by performing a mass-energy balance on the burner, while the burner total pressure, p_h, was measured and the summation of supply gas flow rates, W_h, were determined. The equivalence ratio, ϕ, quantifies the amount of fuel injection based on the oxygen content of the burner-nozzle exit flow (or combustion entrance flow). The fuel injection total pressure, p_f, was used to calculate the dynamic pressure ratio, q_r, (obtained duct dynamic pressure from theory) used in equation (1).

TABLE II. - TEST SUMMARY

RUN	T_t K	p_h MN/m^2	W_h Kg/s	ϕ_1	ϕ_2	p_{f_1} MN/m^2	p_{f_2} MN/m^2	COMMENTS
415-2	1670.	2.19	3.30	0	0	——	——	——
415-3	1610.	2.19	3.30	.26	0	1.61	——	——
415-4	1670.	2.22	3.29	0	.78	——	2.26	——
415-5	1580.	2.20	3.36	.23	.72	1.62	2.30	PITOT PRESS
415-6	1690.	2.23	3.32	.30	.76	1.62	2.28	GAS SAMPLE
415-7	1640.	2.21	3.34	.21	.72	1.67	2.28	GAS SAMPLE
415-8	1690.	2.24	3.31	.23	.74	1.63	2.24	GAS SAMPLE
415-9	1680.	2.23	3.33	.24	.74	1.61	2.28	GAS SAMPLE
416-8	2140.	2.08	2.63	0	0	——	——	——
416-10	2190.	2.11	2.56	0	1.05	——	1.76	PITOT PRESS
416-11	2220.	2.04	2.52	0	.99	——	1.76	GAS SAMPLE
416-12	2170.	2.06	2.61	0	.96	——	1.76	GAS SAMPLE
416-13	2110.	2.10	2.70	0	.97	——	1.71	GAS SAMPLE
416-14	2080.	2.09	2.70	0	.90	——	1.70	GAS SAMPLE

Results from these tests are compared with the one-dimensional theory described in the Analysis section. In order to apply the theory, nominal burner conditions were established from the data as shown in table III.

TABLE III. – NOMINAL BURNER CONDITIONS

	BURNER CONDITION	
	1	2
T_t, K	1680	2100
p_h, MN/m^2	2.21	2.08
W_h, Kg/s	3.30	2.54

With these nominal burner conditions and the nozzle exit to throat area ratio, the combustor initial flow properties (or nozzle exit flow properties) were determined and are presented in table IV. Using these properties and the fuel reaction distributions described in the Analysis section, the theoretical calculations were made. The theory is compared to the measured wall static pressure distributions, local heat flux distributions, and integral properties of the combustion duct exit flow in the following sections.

TABLE IV. – INITIAL FLOW PROPERTIES FOR

ONE-DIMENSIONAL THEORY

	BURNER CONDITION	
	1	2
Mach Number	2.77	2.72
Static Pressure, N/m^2	77630.	72610.
Static Temperature, K	780.	1045.

Wall Static Pressure

Burner condition 1.- Wall static pressures measured along the combustion duct centerline are presented for first-stage, second-stage, and two-stage hydrogen fuel injection in figures 6, 7, and 8, respectively. Data are shown in all three figures for zero fuel injection ($\phi_1 = 0$) as a baseline for comparison with fuel injection data. The zero fuel data in the constant area section and in the last half of the diverging section compare well with the one-dimensional theory. In the first half of the diverging section, the high top wall pressures as well as the general waviness of the entire pressure distribution were probably caused by the non-smooth combustor walls and the general three-dimensional effects. The top and bottom walls are an assembly of sections having hinge joints and inserted blocks (see figs. 3 and 4), which cause some physical misalignments. In support of this it was discovered that the second-stage fuel injector block was recessed .05 mm into the duct wall. The actual flow is also not one-dimensional, as will be seen in the discussion of the exit flow measurements later. These discontinuities in the walls and the three-dimensional effect cause shock and expansion waves which probably contributed to the observed waviness of the pressure distribution. The pressure measured in the nozzle near the exit is high compared to the theory ($p/p_h = 0.0370$) probably due to the non-aerodynamically smooth interior surface of the burner nozzle. The high temperature zirconium surface coating is rather rough in texture and has local dimples at the pressure orifices which could make the true static pressure difficult to obtain. Overall agreement between the zero fuel injection pressure distribution and the one-dimensional theory is satisfactory.

When fuel is injected in the first-stage with overall equivalence ratio of 0.26, it is seen that the pressure data are nearly the same as without fuel injection. The most significant pressure rise occurs just downstream of the first-stage. Within the accuracy of the measurements, the pressures upstream of the first-stage injection are essentially unchanged compared to the zero fuel injection case. The increased pressure in the injector region is caused by the entering duct flow behaving as if the fuel jet and associated heat release was an equivalent solid body obstruction. The obstruction causes local nonuniformities such as shocks and expansions of various strengths and local boundary layer separations. One-dimensional theory, however, shows a larger increase in pressure compared to the data. This suggests that the heat release due to combustion is greatly delayed in this combustion data as compared to the theoretical mixing model. It is believed that the fuel remained near the highly cooled walls, which resulted in the failure of the fuel to achieve the temperature required for ignition. The one-dimensional theory assumes chemical equilibrium and would not predict delayed ignition. The increase in the theoretical pressure distribution level for fuel injection with no reaction, compares favorably with the increase in the data indicating that the fuel injected in the experiment did not burn appreciably.

The second-stage fuel injection data shown in figure 7, clearly indicate the occurrence of some combustion as the data are midway between the theoretical curves for injection with and without reaction. The pressure rise begins approximately two duct heights downstream of the second-stage injector and is more gradual than that predicted by the theoretical mixing model. (See eq. (3).)

12

This delay in pressure rise may be due to an ignition delay phenomenon, whereas the subsequent gradual pressure rise may be a result of the presence of an initially favorable pressure gradient reducing the mainstream turbulence. (See ref. 11.) In the case of the nonreactive mixing data correlation, the test had a slightly adverse pressure gradient.

In figure 8, two-stage fuel injection results indicate a much greater change in the internal duct flow as compared to the results for injection in single stages. (See figs. 6 and 7.) From previous tests the flow was expected to be highly nonuniform and three-dimensional in nature. With the aid of labeled focal points of attention in figure 8(a), the results are subsequently discussed. At point 1, the sharp pressure rise indicates the presence of a shock probably caused by flow separation on the top wall due to first stage injection and combustion. Some hydrogen fuel probably circulates forward into the separated region enhancing the shock strength. The measured pressure level behind this shock is small compared to the theoretical normal shock pressure level of $p/p_h = 0.33$. This suggests that the average flow experiences a pressure rise indicative of an oblique shock rather than normal shock and hence the flow remains supersonic. At point 2, the gradual rise in pressure on both walls indicates heat addition in the supersonic flow in this constant area section. At point 3, the pressure rise on the bottom wall indicates the presence of a shock caused by a separated flow ahead of the second stage fuel injection which apparently extends to the beginning of the diverging section. The pressure of reacting hydrogen fuel is also indicated. The separation shock travels across the duct to the top wall and is sensed as indicated at point 4. This indicates that the flow is still generally supersonic and has no dominating local subsonic flow regions at the beginning of the diverging section. The subsequent gradual pressure drop at point 5 indicates that the flow is still supersonic and the effects of the diverging duct geometry dominate over the effects of the continuing heat addition. The theory in this case predicted a lower initial pressure rise since it does not include shocks and flow separations. It is interesting to note that the fuel injection in the first-stage (see fig. 6) did not appear to burn. However, when the second stage was turned on (see fig. 8(a)) a strong interaction occurred which promoted first, as well as second-stage combustion. These data, including the specific features discussed above, were repeatable as shown in figure 8(b).

Burner condition 2.- Compared to burner condition 1, this case uses a burner test gas having reduced oxygen content, increased total temperature, and reduced dynamic pressure for the purpose of simulating the effect of first-stage combustion infinitely far upstream. As used here, infinitely far upstream means that the flow is uniform at the second-stage injector location. The burner total pressure was adjusted to give the same dynamic pressure at the second-stage injector, as was theoretically computed to have existed in the two-stage injector test with burner condition 1.

The essence of the test program as originally conceived was to determine the effect of nonuniformity across the duct flow on the combustion of second-stage fuel. The nonuniform and uniform duct flow results are presented in figures 8(a) and 9, respectively. It should be noted that the relative amount of fuel injected into the combustion duct at the second-stage is the same in

13

both of these tests, even though the equivalence ratios are different. In both cases the second-stage fuel was nominally enough to use the remaining oxygen assuming complete first-stage combustion. For burner condition 1, the test gas has oxygen content by volume equal to that of air; and for burner condition 2, the oxygen content is reduced to 77 percent that of air.

In figure 9, the results are similar to those presented in figure 7. Again, the pressure rise was delayed at least two duct heights and the data near the exit are also midway between the theory with and without reaction. In comparing figures 8(a) and 9, it is apparent that when the fuel injection stages are closer together, as in figure 8(a), there occurs a favorable stage interaction which suggests greater mixing and combustion of the fuel. This stage interaction effect is further analyzed in the discussion of the exit probe rake measurements.

Wall Heat Transfer

Measurements were made of both local heat transfer distribution on the duct bottom wall and the overall duct heat transfer as described in the Instrumentation section. To check the distribution obtained, the local heat transfer rates were integrated over the wetted internal duct area. In performing the integration, local heat transfer rates were adjusted for differences between wall thermocouple temperatures and backside water cooling temperatures on the top and bottom walls. Using these temperature differences as a guide, the bottom wall heat transfer was estimated to be greater than the top wall heat transfer by the percentages given in table V.

TABLE V. – COMPARISON OF INTEGRATED, MEASURED, AND THEORETICAL

COMBUSTION DUCT BULK HEAT TRANSFER

Run	Burner Condition	Fuel Injection Stage	Bottom Wall Higher than Top by (%)	Bulk Heat Transfer MJ/sec		
				Integrated from Local Values	Measured Overall	Theory
415-2	1	None	6	.324	.276	.287
415-3	1	First	14	.300	.310	.436
415-4	1	Second	14	.546	.471	.486
415-5	1	Two	14	1.001	.970	.481
416-8	2	None	8	.414	.374	.319
416-12	2	Second	28	.509	.496	.422

It is believed that the heat transfer is greater on the bottom wall because of the greater wall roughness caused by inserted blocks not present in the top. (See figs. 3 and 4.) In table V, the resulting integrated values are compared to the bulk measured values and are in good agreement. These are then compared with results of the one-dimensional theory, which employs a Reynold's analogy model modified for adverse pressure gradient effects. The fact that the theoretical results were high for run 415-3 and low for run 415-5 will subsequently be discussed.

Theoretical computation of heat transfer requires selection of realistic input values for the average skin friction coefficient and wall temperature. The average skin friction coefficient selected was 0.0026. The wall temperature selected as input to the theory was a constant 370 K for all cases. Wall thermocouple measurements indicated temperatures from 340 to 500 K. The use of the constant value introduces errors in the computed heat transfer of somewhere between 2 percent higher to 10 percent lower than if the actual wall temperature had been used.

Burner condition 1.- The heat transfer measured along the bottom wall of the combustion duct is presented for the first-stage, second-stage, and two-stage injection in figures 10, 11, and 12, respectively. Data are shown in all three figures for zero fuel injection as a baseline for comparison with fuel injection data.

In figure 10, the zero fuel injection data compare favorably with the theory indicating that the selection of skin friction coefficient and wall temperature previously mentioned was satisfactory for the baseline case. Comparing data with and without injection, indicates an insignificant effect of fuel injection on heat transfer – an observation consistent with results of the pressure distribution. (See fig. 6.) The theory showed a high heat transfer level in the constant area section due to the adverse pressure gradients and dropped down as the theoretical calculation proceeded into the diverging section. It was also unusual not to observe an increase in the heat transfer data at the first-stage injector location caused by local shocks in front of the perpendicularly injected fuel jet. This was observed in other data to be presented next in figures 11 and 12.

In figure 11, the data trend for second-stage injection appears similar to that of the corresponding pressure distribution in figure 7. The high heat transfer observed at the injector block is probably due to shocks and flow separation, as was expected. Downstream of this point the theory and data follow similar trends, although the theory is slightly below the data. Downstream of the second-stage injector, the heat transfer (as estimated from wall temperature distribution) was higher on bottom wall than the top wall. This is one possible reason why the bottom wall heat transfer data were higher than predicted by theory.

In figure 12, the two-stage heat transfer data are quite high compared to the theory. This is similar to the corresponding pressure data in figure 8(a). It should be noted that the heat transfer measured at $x/H_i = 0.4$ was the same with and without injection indicating that the flow separation discussed in figure 8(a) did not propagate upstream to this point. Again the characteristically

high heat transfer level at the first-stage fuel injector was observed followed by a drop in level, as was shown in figure 11. It is believed that the failure of the theory to predict the high heat transfer data occurred because the theory did not calculate the high mass flux which resulted from the reduction of the effective duct flow area due to flow separation. The peak in the theoretical heat transfer level at the second-stage injector resulted from the presence of an adverse pressure gradient in the theory. Its shape results from the step-wise nature of the theoretical calculation.

Burner condition 2.- Heat transfer data for second-stage injection into the duct flow which has uniformly reduced oxygen content, are shown in figure 13. As expected the data trend is similar to that of figure 11, but there are some differences. The difference between the zero injection data and the theory is greater than in figure 11. Also, the theoretical results with fuel injection for burner condition 2 are only 10 percent higher than those for burner condition 1. This can be explained by the fact that although there was a large increase in total temperature, which tended to increase the heat transfer, this was counteracted by a decrease in the mass flux. At the duct exit, the measured heat transfer rates with injection are twice as large as without injection, while in figure 11 they are three times as large. This indicates that the second-stage fuel in figure 13 may be burning less than in figure 11 due to the reduced oxygen content of the duct flow. The theory predicts lower heat transfer in the diverging portion of the duct than was the case in figure 11, because the theo-retically calculated pressure gradient was near zero. (See fig. 9.)

Instream Pitot Pressure and Gas Composition

Pitot pressure and gas composition are presented only for the case of two-stage injection where the initial duct flow contained an oxygen volume fraction equal to that of air, and second-stage injection where the volume fraction of oxygen was reduced to 77 percent of the air value.

Burner condition 1.- Horizontal profiles at the duct exit of pitot pressure, local equivalence ratio, combustion efficiency, and local fraction reacted at four vertical locations are presented for the case of two-stage injection in figures 14 through 17. This presentation is followed by a discussion of the related contour maps of pitot pressure, local equivalence ratio, and local fraction reacted at the duct exit given in figure 18.

In figures 14 through 17, the pitot pressure was laterally uniform near the bottom wall but became somewhat undulatory with increasing vertical height. The average level of each profile also increased with increasing vertical height. Using the theoretical static pressure and Mach number, the average pitot pressure at the duct exit was calculated to be $p_2/p_h = 0.26$ and compared to the measured profiles in figures 14 through 17. Because pitot pressure is an insensitive and therefore poor indicator of the amount of fuel locally present in the flow, it is necessary to examine the measured fuel distribution via the gas sample results. In these same figures the local equivalence ratio, which quantifies the degree to which the fuel mixture is fuel-lean or fuel-rich, is shown to be fairly uniform laterally with a centerline peak value which is about 15 percent greater than

the profile average. Near the bottom wall (from which the majority of the fuel
was injected) the flow is fuel-rich ($\phi > 1$), while the mixture tends to become
fuel-lean ($\phi < 1$) with increasing vertical height. The bulk injected value is
shown on each figure and is different for each vertical location of the probe,
since only one vertical location could be measured per test run. Although the
variation in the bulk injected values was 10 percent, this effect was not
eliminated by nondimensionalizing the local ϕ_ℓ values. The reason for this

was that the variation in the fuel distribution was far greater than the bulk
variation. This can be seen by comparing the profile magnitudes in figures
15 and 17. The bulk values are essentially equal at 0.93 and 0.95, respectively.

The pitot pressure is expected to be sensitive to equivalence ratios less
than one, where the total pressure losses due to heat addition vary more directly
with fuel content. Interestingly, figure 19 shows the pitot pressure to be
completely insensitive to magnitudes of local equivalence ratio greater than
one. In spite of this insensitivity, the pitot pressure qualitatively responds
inversely to changes in the local equivalence ratio trend. This feature is use-
ful in checking or filling in gaps of the fuel distribution shape. After the
fuel distribution, the next most important information is the combustion effi-
ciency and local fraction reacted.

Combustion efficiency is simply a measure of the relative amounts of un-
reacted hydrogen and oxygen coexisting in the gas sample as collected by the
pitot probe rake and is defined according to which reactant is the limiter.
When the equivalence ratio is less than one, the combustion efficiency equals
the mass ratio of reacted hydrogen to total hydrogen. When equivalence ratio is
greater than one, it equals the ratio of reacted oxygen to total oxygen, where
these totals equal the addition of mass of the specie in the reacted and unreacted
states. Coexistence of reactants in the gas samples can be caused by two phe-
nomena. The first phenomenon, which is related to the chemistry of the flow, is
finite rate reactions, that is, the reactants are in intimate molecular contact
but the reaction is proceeding at a slow pace. The internal-expansion pitot
probe is designed to quench the entering gas; hence, the reactants would be co-
existing in the sample bottle. The second phenomenon, which is related to the
turbulent nature of the flow, is unmixedness. (See ref. 12.) Unmixedness occurs
when the probe is positioned in the center of the turbulent reaction zone where
there are no steady streamlines in the laminar sense. Lumps or turbules of un-
reacted hydrogen and oxygen are being transported in a random manner in this
zone. Therefore, it is conceivable that alternately unreacted hydrogen and oxygen
lumps could enter the probe and be quenched with reactants coexisting in the
sample bottle. As seen in figures 14 through 17, the combustion efficiency is
virtually unity when the probe is not in the intense reaction zone (that is, where
$\phi = 1 \pm 0.3$.) This implies that phenomena of finite rate reactions and unmixed-
ness do not exist there and the flow is considered to be in chemical equilibrium.
In regions of the flow where $\phi = \pm 0.3$, the combustion efficiency invariably
decreases, which indicates that finite rate reaction and/or unmixedness are factors
to be considered. Figure 20, dramatically illustrates this effect in a form that
may be useful in theoretical modeling studies of turbulent reacting flowfields
such as in reference 13. It is suggested that the magnitude, extent, and shape
of this data correlation may be related in some way to the general nature, scale,
and intensity of the flow turbulence. This effect was also measured in reference

14. The proportion to which these two phenomena contribute to the decrease in combustion efficiency was not resolved in the experiment. This behavior of the combustion efficiency is useful in checking the data reduction to local equivalence ratio values.

The local fraction reacted, F, equals the combustion efficiency when $\phi \leq 1.0$. When $\phi \geq 1.0$, F equals the local ratio of combustion efficiency to equivalence ratio. When the local fraction reacted is adjusted to a local combustion efficiency of one (see dashed line, F_c, figures 14 through 17), then F_c has the same definition as the mixing efficiency used in the one-dimensional theory which is based on the non-reactive mixing data correlation. The reason for assuming $\eta_c = 1.0$ is that the assessment of the effects of unmixedness or finite rate reactions was not possible in the non-reactive test data. The difference between the local fraction reacted profiles assuming the measured η_c and $\eta_c = 1$ (in figures 14 through 17, the data compared with the dashed line) is a measure of the effect of unmixedness/chemical kinetics on the amount of fuel burned. Note that the local fraction reacted, F, cannot be integrated to give an average value, but is nevertheless a useful indicator for local conditions only. The comparison of the integral values at the duct exit is discussed at the end of this section.

As shown in figures 14 through 17, the local fraction of fuel reacted, F, consistently drops in the middle as ϕ increases, which is expected by definition. The mixing efficiency of 0.49, obtained from an empirical mixing model, is lower than the adjusted F_1 combustion data profile. The combustion data are higher probably because of the strong stage interaction discussed in figure 8. The effects of the separated boundary layers on the mixing efficiency were not modeled in the theory.

In figure 18, these profile results are presented pictorially in the form of constant value contour maps for pitot pressure, local equivalence ratio, and local fraction of fuel reacted. The discussion is basically the same because the contours were cross plotted from the profiles, but this presentation provides greater physical insight. The contours form horizontal layers of increasing pitot pressure, decreasing equivalence ratio, and increasing local fraction reacted as the height increases. Most of the fuel is near the lower wall of the combustion duct, indicating that the second-stage fuel did not penetrate as far as expected. Again, it is evident that the pitot pressure is an insensitive indicator of fuel distribution magnitude, but does indicate gross trends. The approximate area-weighted integral values of p_2/p_h, ϕ, η_r, η_m are 0.22, 1.17, 0.745, and 0.760, respectively. (Note that η_r and η_m are the integral values that correspond to the local values of F and F_1.) These values are only gross estimates because they should have been integrated by mass flux weighting. Mass flux weighting was not performed because the variation of the static pressure was not measured across the duct exit and strong variation was expected (see reference 15 for a typical static pressure variation across a non-reacting mixing zone.) These integral values will be further discussed at the end of the discussion on the burner condition 2 exit profile results.

18

Burner condition 2.- Horizontal profiles at the duct exit at four vertical locations are presented for the case of second-stage injection in figures 21 through 24, followed by the contour maps in figure 25. In figures 21 through 24, the pitot pressure profile was found to be highly nonuniform. The local equivalence ratio profile readily shows the inverse profile shape compared to the pitot pressure profile shape. The equivalence ratio variation in figure 23 is approximately a factor of three with the peaks at $\phi \approx 5$, indicating very poor mixing. It should be noted that for points where $\phi = 1 \pm 0.3$, the combustion efficiency drops. The local fraction of fuel reacted is naturally quite low where the equivalence ratio is high by definition.

Figure 25, definitely aids in visualizing the flowfield, though not without some error. Note particularly the contour shape and number of peaks. The fuel distribution is not nearly as uniform as the two-stage results presented in figure 18. The fact that four peaks are detected is surprising, since fuel was injected from six equally spaced holes. Two explanations are apparent. First, the second-stage injector jets number 2 and 3, as well as, 4 and 5 may have merged due to some three-dimensional effect near the injectors, thereby providing four peaks at the exit. This is made plausible because the injector jets 1 and 6 seem to have gravitated toward the side walls instead of tracking directly downstream of their respective injector holes. Second, and considered more likely, the data mesh may be too large to detect the peaks from jets 2 and 4, as these would have occurred midway between two pitot probes as can be seen in figure 23 (also see six distinct fuel-rich core regions in figure 26(b), to be discussed later.) In general, the contours are only as accurate as the data grid size allows.

In the case shown in figure 18 the grid size was adequate, but in figure 25 it is apparent that a fine grid was necessary for proper resolution. Hence, the use of a large data grid and linear interpolation between data points in the profiles to produce the contour map can be misleading, but can be expected to present the gross features of the flow fairly well. With this in mind, the area-weighted values for p_2/p_h, ϕ, η_r, η_m, are 0.22, 1.70, 0.420, and 0.430. The significance of these values for burner conditions 1 and 2 are presented next.

Table 6 summarizes the comparison of the data with the theory for some integral flow properties at the combustion duct exit. The comparison includes both the two-stage test (burner condition 1) and the second-stage test (burner condition 2). The integral flow properties consisting of p_2/p_h and ϕ for the data, were obtained by area-weighting the local flow property values as presented in figures 18 and 25. The integral reaction efficiency, η_r, and the integral mixing efficiency, η_m, were obtained using equations (4) and (5), respectively. The contours for the integrand properties are not reported herein.

$$\eta_r = \frac{\int_A \alpha_{H_2,r} \, dA}{\int_A \alpha_{H_2} \, dA} \tag{4}$$

$$\eta_r = \frac{\int_A \alpha_{H_2,r}\, dA}{\int_A \alpha_{H_2}\, dA} \tag{5}$$

TABLE VI. – COMPARISON OF INTEGRAL DATA AND THEORETICAL

PROPERTIES AT THE COMBUSTION DUCT EXIT

Burner Condition	1		2	
Fuel Stages	Two		Second	
	Data	Theory	Data	Theory
P_2/P_h	0.22	0.26	0.22	0.22
ϕ	1.17	1.00	1.70	1.00
η_r	0.745	0.490	0.420	0.540
η_m	0.760	0.490	0.430	0.540
f	-2	0	-2	0
$(\eta_m)_2$	0.680	0.340	0.430	0.540

For equivalence ratio, the data are high as a result of the area-weighting procedure which assumes that the mass flux is constant across the duct exit. Actually, lower mass flux values would be expected in the high equivalence ratio regions because of the low molecular weight of hydrogen. If the integral of ϕ_ℓ had been weighted by the mass flux, then the integral value would be lower, which would more closely agree with the theory or bulk value. The high second-stage equivalence ratio of 1.70 indicates that very large static pressure variations must have occurred. The static pressure variations are probably greater in this case as compared to the more uniform two-stage case. It should be noted that due to unmixedness and/or kinetics, the experimental values for η_r are slightly lower than η_m. A measure of this effect is provided for by use of an integral unmixedness/kinetics factor, f, which is computed using the following equation:

$$f = \left(\frac{\eta_r - \eta_m}{\eta_m}\right) 100 \text{ percent} \tag{6}$$

This factor, f, provides a percentage correction to the cold flow mixing theory in order for the theory to better predict such behavior for similar fuel injection configurations. The fact that f is small (see table VI) indicates that the unmixedness/kinetics effects are insignificant at the combustion duct exit.

A measure of the energy release efficiency of the second-stage fuel is the fraction of second-stage fuel mixed $(\eta_m)_2$, which is computed using the following equation:

$$(\eta_m)_2 = \frac{\eta_m \left(\phi_1 + \phi_2\right) - \phi_1}{\phi_2} \qquad (7)$$

In table VI, the integral data values for $(\eta_m)_2$ show that 60 percent more second-stage fuel burned in the two-stage test than in the single second-stage test. The combustion of first- and second-stage fuel apparently interacted through an extensive flow separation, which promoted the mixing and combustion of the second-stage fuel. In table VI, the theoretical value, $(\eta_m)_2$, is lower for the two-stage test as compared to the second-stage test, which is a result of the theoretical mixing model development. For two-stage injection, the $(\eta_m)_2$ experimental value was twice the theoretical. This indicates that twice as much fuel was burned in the experiment as compared to the theoretical prediction. This result is also supported by the previous comparison of measured wall static pressure distribution (see fig. 8(a)) and the heat transfer distribution (see fig. 12) with theory.

For the second-stage fuel injection test, the $(\eta_m)_2$ experimental value was 80 percent of the theoretical value. This trend is consistent with the pressure and heat transfer distributions shown in figures 9 and 13, respectively, where the data are lower than the theory.

Photographs

The quantitative results previously discussed established some understanding of the fuel injection performance in the combustion duct. Evaluation of some additional qualitative results may add to further understanding. Figure 26(a), (b), and (c) are photographs of the burner condition 1 duct exit flow for first-stage, second-stage, and two-stage injection, respectively. In figures 26(a) and (b), the first-stage injector hole size is larger than reported herein, while the second-stage injector hole size is the same as previously reported. Figure 26(a) shows qualitatively that even if the first-stage fuel does not burn appreciably in the duct, it certainly burns rapidly at the exit where the emission of light (visible flame due to sundry chemical impurities present) stops short in the view. This indicates that the fuel was well mixed at the duct exit. The continuous emission intensity also indicates that the fuel was evenly distributed. In figure 26(b), the second-stage injection results are shown for the data presented in figures 7 and 11. Based on the similarity of results presented in figures 7 and 9, it can be assumed that figure 26(b) also represents the general features of second-stage with burner condition 2 as well. Note the stratified emission intensity in this case. The six dark streaks indicate fuel-rich regions downstream of six injectors which were measured to be a maximum of $\phi \approx 5$, while the brighter bands are regions where intense combustion is occurring. The observation of these six fuel-rich regions

indicates that fuel jets did not merge, but rather the probe rake data apparently failed to resolve all of the fuel-rich regions because of the large spacing of the probes. The stratified emission and the long distance downstream before emission ceases, suggests that the second-stage fuel is mixing slower than that of the first stage. This is consistent with the probe results. The two-stage results shown in figure 26(c) indicate the flow was well mixed and emission terminates in view, indicating that the integral of fraction of fuel reacted was probably closer to one than in the second-stage case. This supports the quantitative results.

CONCLUSIONS

Investigation of the effects of combustion duct flow nonuniformity on second-stage hydrogen fuel injection, and subsequent mixing and combustion has been discussed. Additional single stage fuel injection results were also discussed.

From data analysis, the following conclusions are made:

Based on wall static pressure and heat transfer distributions,

(1) first-stage fuel injected by itself apparently did not burn, as no changes were detected in the wall static pressure or heat transfer rate distributions;

(2) second-stage fuel injection by itself burned at a rate less than that estimated from the nonreactive mixing correlation,

(3) two-stage fuel injection produced a large interaction between the stages probably due to extensive flow separations and oblique shock waves,

(4) second-stage fuel injection into a uniform duct flow, which simulated first-stage fuel combustion infinitely far upstream, produced results similar to (2) above, but with less reaction due to the lower oxygen content,

(5) heat transfer predictions were satisfactory except where extensive flow separations occurred or where the fuel apparently failed to ignite,

Based on instream measurements:

(1) Effect of unmixedness/chemical kinetics on the amount of fuel burned was found to be insignificant at the combustion duct exit.

(2) Twice the amount of second-stage fuel burned in the two-stage test compared to the amount predicted to burn based on an empirical nonreactive mixing correlation. This indicates that in the mixing model development, the second stage may have been reduced too much.

(3) Sixty percent more second-stage fuel burned when injected into a nonuniform duct flow as compared to injection into a uniform duct flow.

22

apparently this is a result of the interaction between the fuel injection stages characterized by local flow separation.

RECOMMENDATIONS

(1)   Instream measurement of static pressures at the combustion duct exit would permit calculation of Mach numbers. Mass flux distributions could then be determined by using either a measured or calculated temperature. This would permit computing exit mass flow balances and mass weighted integral property values.

(2)   Additional work is required to determine the extent to which unmixedness contributes to the observed decrease in combustion efficiency in the intense combustion zone. Use of a blunt-nosed probe, as in reference 15, would permit completion of the reaction of molecularly mixed reactants as the gas enters the probe. Hence, the coexistence of hydrogen and oxygen found in the gas sample would then be due only to unmixedness.

(3)   There is a need to develop two-and three-dimensional theories that will include shock waves and flow separations. These improved theories should allow more realistic prediction of the exit flow profiles, wall pressure distributions, and particularly the wall heat transfer distribution.

(4)   Additional work is required to understand the phenomena of fuel ignition as related to the duct flow total temperature and the fuel injection - duct flow interaction.

(5)   Further work is required to understand the mechanism of the strong interaction between fuel injection stages.

REFERENCES

1. Henry, J. R.; and McLellan, C. H.: Air-Breathing Launch Vehicle for Earth-Orbit Shuttle - New Technology and Development Approach. J. Aircraft, vol. 8, no. 5, May 1971, pp. 381-387.

2. Becker, John V.: New Approaches to Hypersonic Aircraft. Paper presented at Seventh Congress of International Council of Aeronautical Sciences (Rome, Italy), Sept. 1970.

3. Henry, John R.; and Beach, H. Lee: Hypersonic Air-Breathing Propulsion Systems. Vehicle Technology for Civil Aviation - The Seventies and Beyond, NASA SP-292, 1971, pp. 157-177.

4. Henry, J. R.; and Anderson, G. Y.: Design Considerations for the Airframe-Integrated Scramjet. NASA TM X-2895, 1973.

5. Rogers, R. Clayton: Mixing of Hydrogen Injected from Multiple Injectors Normal to a Supersonic Airstream. NASA TN D-6476, 1971.

6. Anderson, G. Y.; and Gooderum, P. B.: Exploratory Tests of Two Strut Fuel Injectors for Supersonic Combustion. NASA TN D-7581, 1974.

7. Rogers, R. C.; and Eggers, J. M.: Supersonic Combustion of Hydrogen Injected Perpendicular to a Ducted Vitiated Airstream. AIAA Paper No. 73-1322, Nov. 1973.

8. Anderson, G. Y.; and Rogers, R. C.: A Comparison of Experimental Supersonic Combustor Performance with an Empirical Correlation of Nonreactive Mixing Results. NASA TM X-2429, Oct. 1971.

9. Russin, William Roger: Performance of a Hydrogen Burner to Simulate Air Entering Scramjet Combustors. NASA TN D-7567, 1974.

10. Eggers, J. M.: Composition Surveys of Test Gas Produced by a Hydrogen-Oxygen - Air Burner. NASA TM X-71964, 1974.

11. Engineering Staff: Hypersonic Research Engine Project-Phase II. Combustor Program, Final Technical Data Report; Doc. No. AP-70-6054 (Contract No. NAS1-6666) AiResearch Manufacturing Co., Mar. 23, 1970. (Also available as NASA CR-66932.)

12. Hawthorne, W. R.; Weddell, D. S.; and Hottel, H. C.: Mixing and Combustion in Turbulent Gas Jets. Third Symposium on Combustion and Flame and Explosion Phenomena, Williams & Wilkins Co., 1949, pp. 226-288.

13. Launder, B. E.; and Spalding, D. B.: Lectures in Mathematical Models of Turbulence. Academic Press, c. 1972.

14. Anderson, G. Y.; Agnone, A. M.; and Russin, W. R.: Composition Distribution and Equivalent Body Shape for a Reacting, Coaxial, Supersonic Hydrogen-Air Flow. NASA TN D-6123, Jan. 1971.

15. Yates, C. L.: Two-Dimensional, Supersonic Mixing of Hydrogen and Air Near a Wall. NASA CR-1723, March 1971.
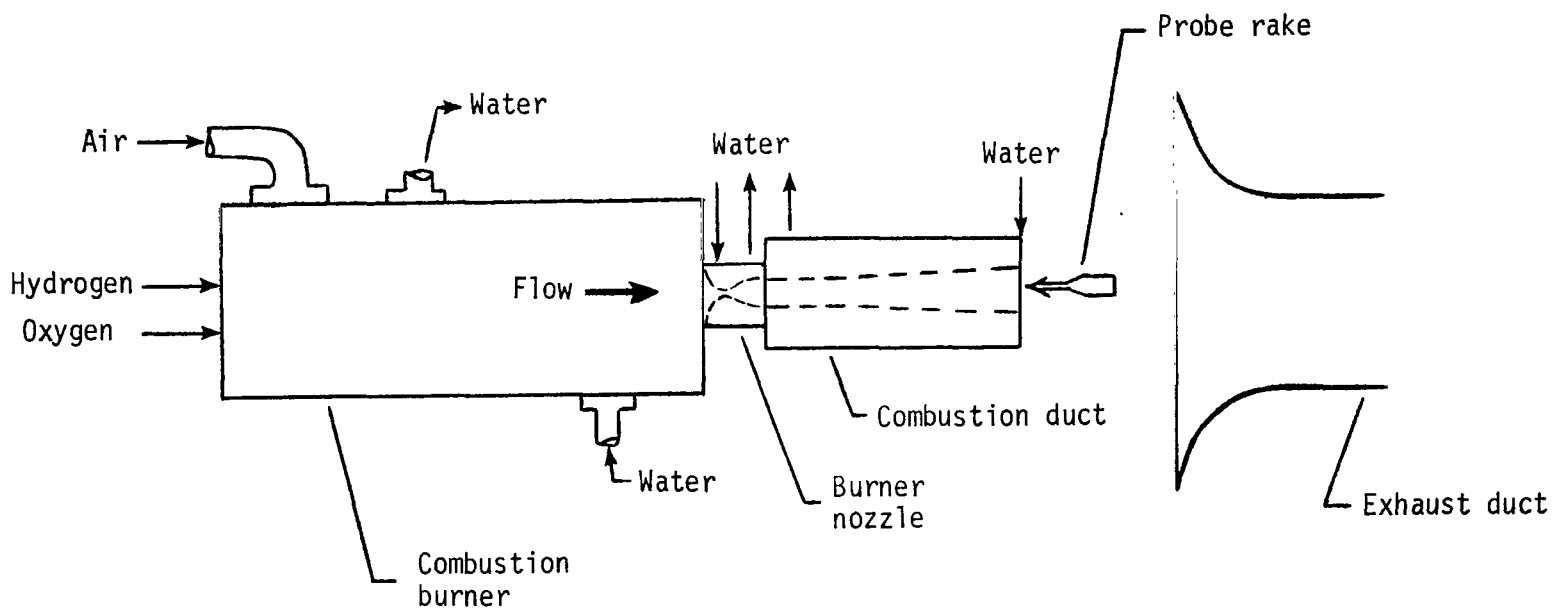
Figure 1.- Experimental test setup.

FLOW →

Z

X

ZIRCONIUM COATED COPPER
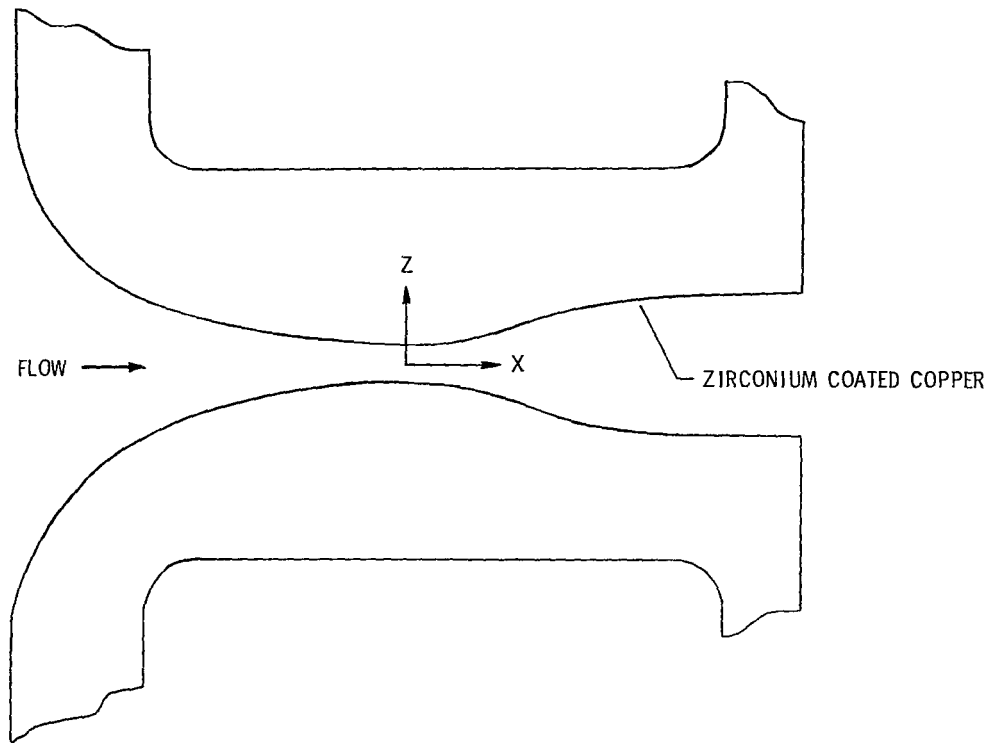
NOZZLE DESIGN CONTOUR			
X (CM)	Z (CM)	X (CM)	Z (CM)
-6.530	1.356	1.138	.742
-6.350	1.303	1.476	.874
-5.715	1.132	1.808	.993
-5.080	.983	2.197	1.120
-4.445	.853	2.664	1.252
-3.810	.744	3.231	1.394
-3.175	.655	3.856	1.521
-2.540	.582	4.242	1.590
-1.905	.523	4.699	1.666
-1.270	.483	4.981	1.707
- .635	.460	5.370	1.753
0.0	.452	5.773	1.791
.165	.452	6.193	1.826
.234	.457	6.614	1.854
.378	.472	7.036	1.875
.538	.505	7.440	1.890
.724	.566	7.811	1.900
.914	.645	8.202	1.905
.945	.660	8.291	1.905

FIGURE 2.- BURNER NOZZLE DESIGN CONTOUR
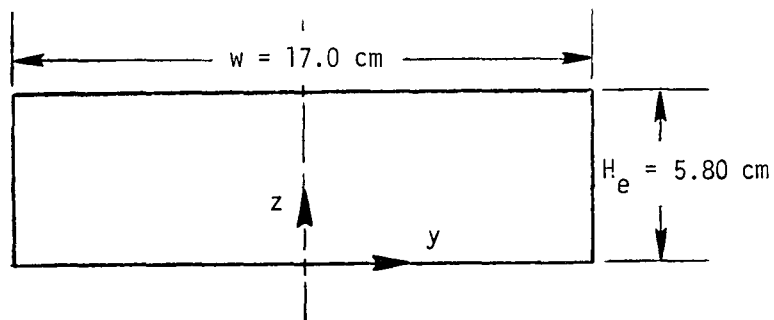
w = 17.0 cm

H_e = 5.80 cm

z

y

.915 cm

.079 cm

(c) Combustion duct exit dimensions and coordinate system

9 probes at 1.905 cm spacing

40°

45° beveled leading edge

.16 cm

Cooling water 4 places

Stainless steel rake strut 1.905 cm thick

Cooling water

(b) Probe tip detail

Instrumentation tubing shield

Instrumentation tubing
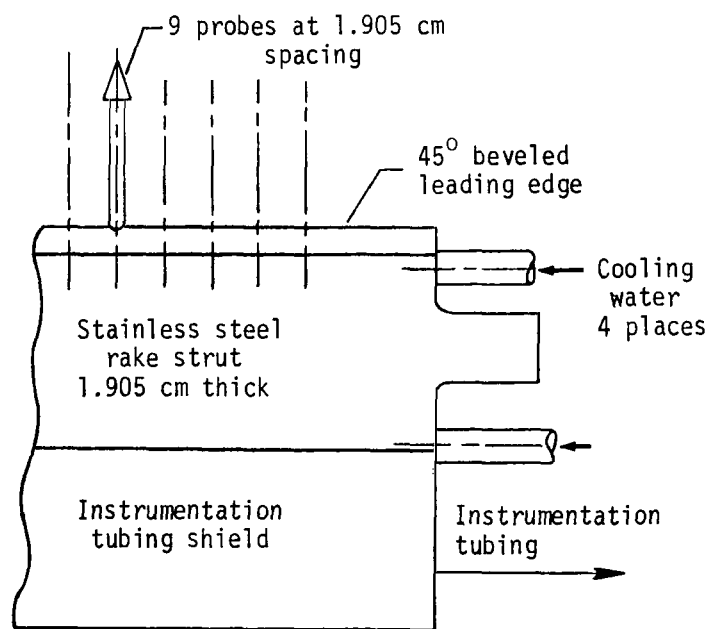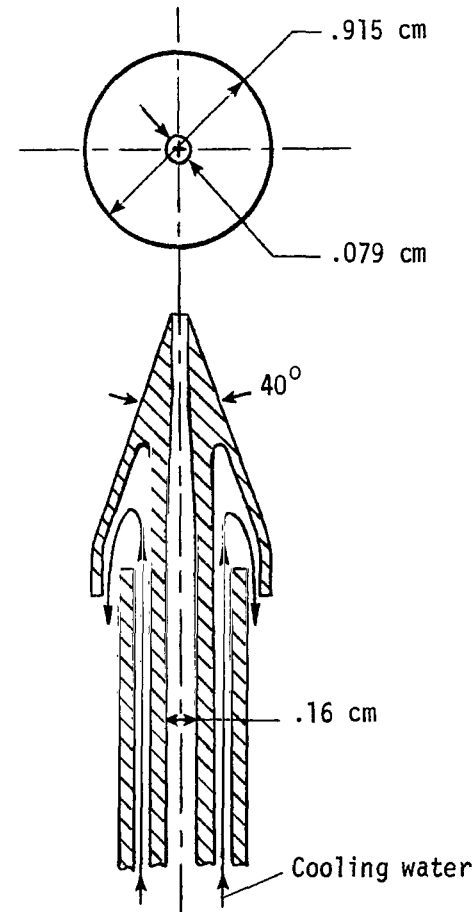
(a) Survey rake

Figure 5.- Survey rake, probe tip detail and combustion duct exit dimensions and coordinate system. (Fig. 2 in ref. 10).
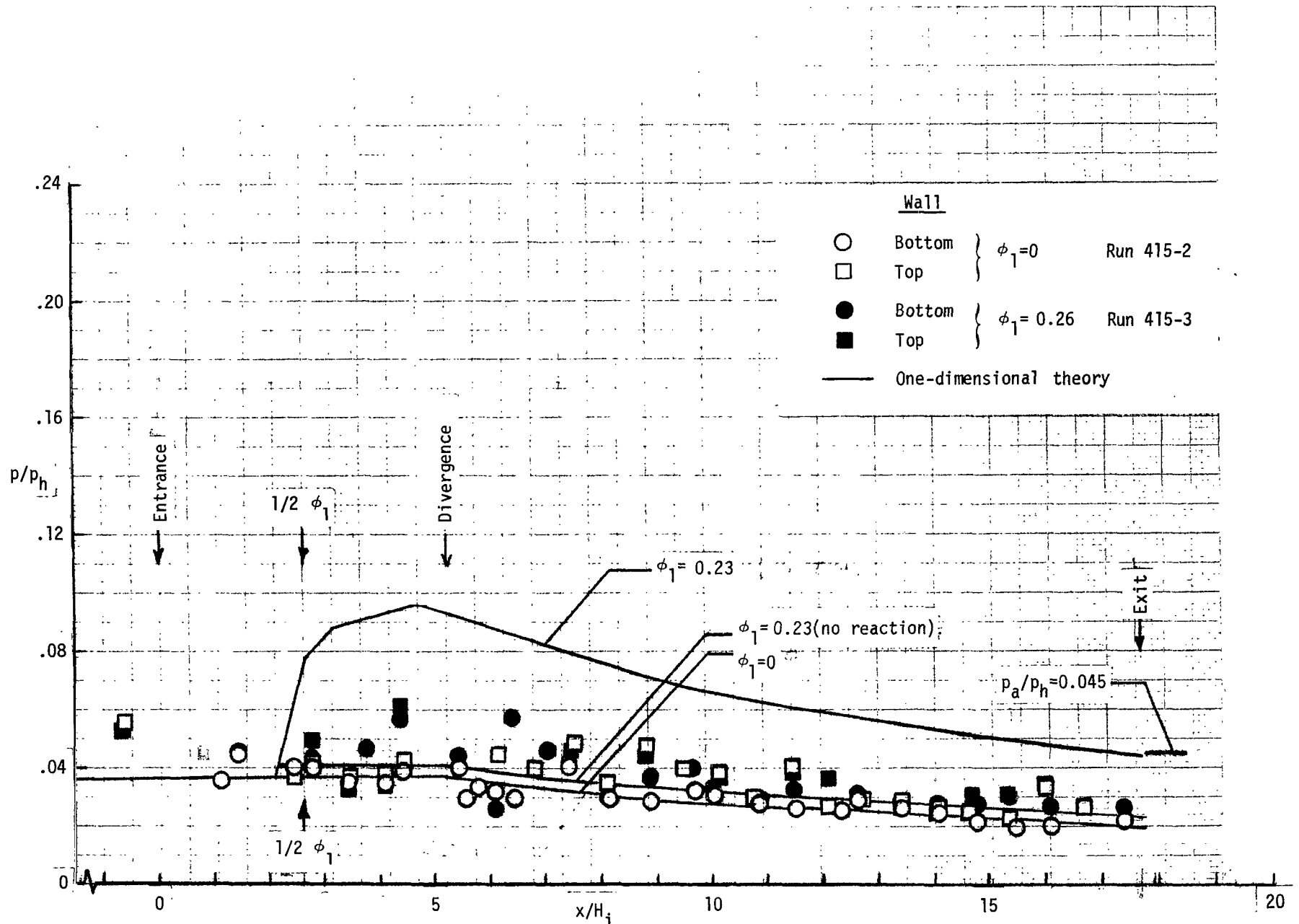
Figure 6.- Burner condition 1, wall pressure, first-stage injection.

First-stage hydrogen
injector block - top wall

.18D

Flow

3.86

5.80

7.3

Second-stage
injector block

Mach
2.75 nozzle

10.2

20.7

47.9

Knuckle
joint

15.7

.18D

2.54

2.80

.38D

3.86

17.0

Bottom wall injector
blocks detail

Combustor cross section at
first-stage injectors
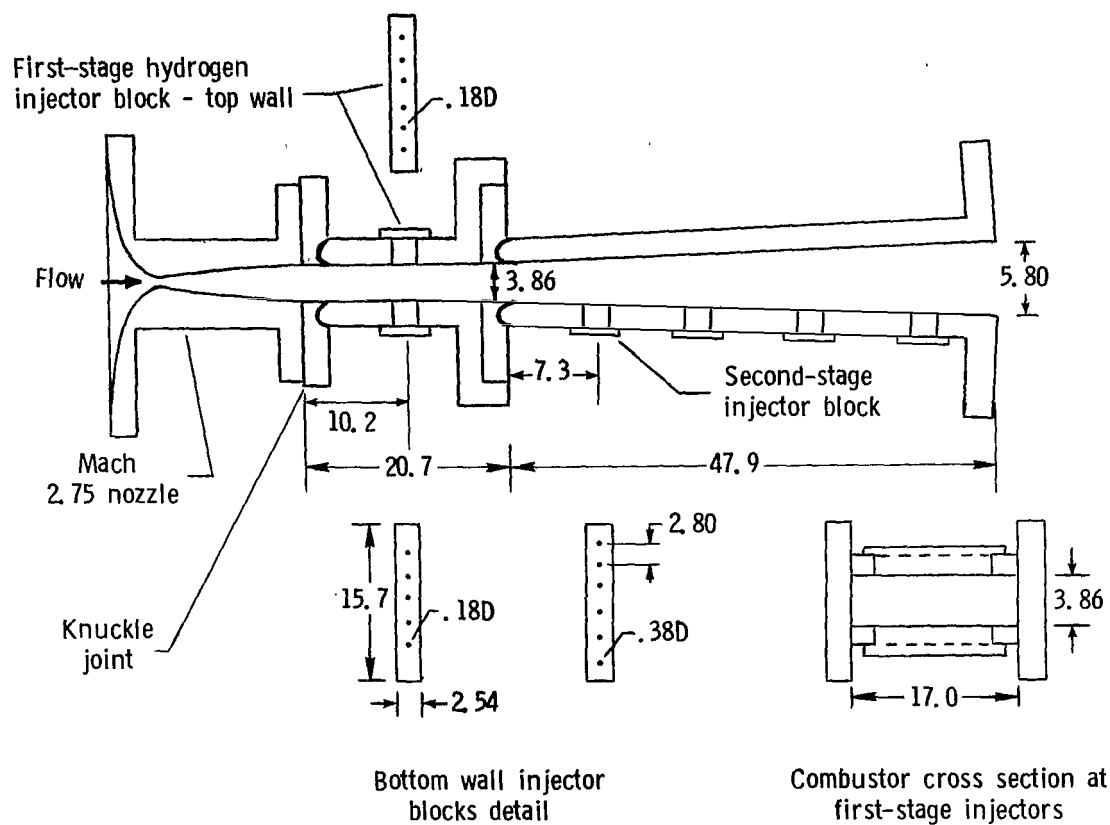
Figure 3.- Schematic of two-dimensional combustion duct. All dimensions are in centimeters.

TOP PLATE   6-24-74

FLOW DIRECTION $\longrightarrow$

BOTTOM PLATE   6-24-74
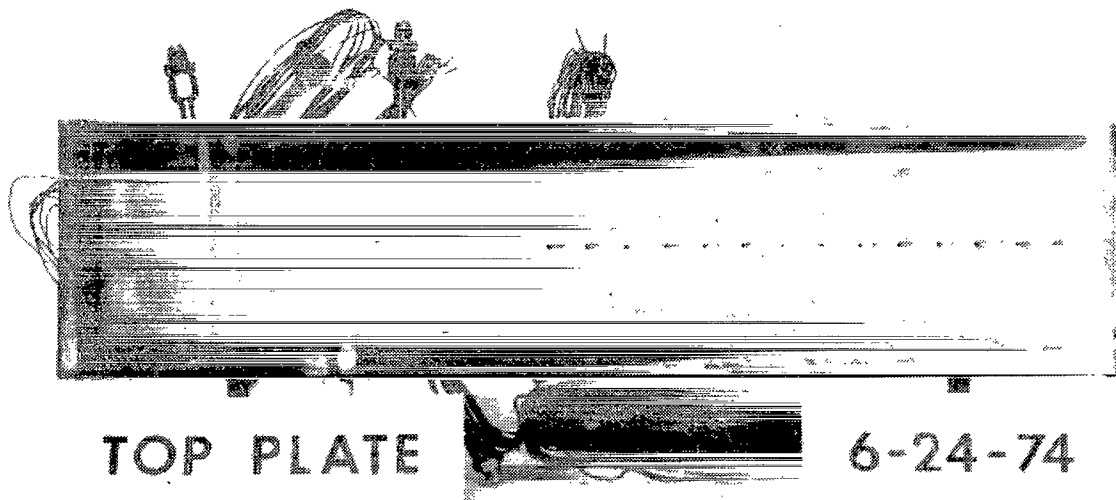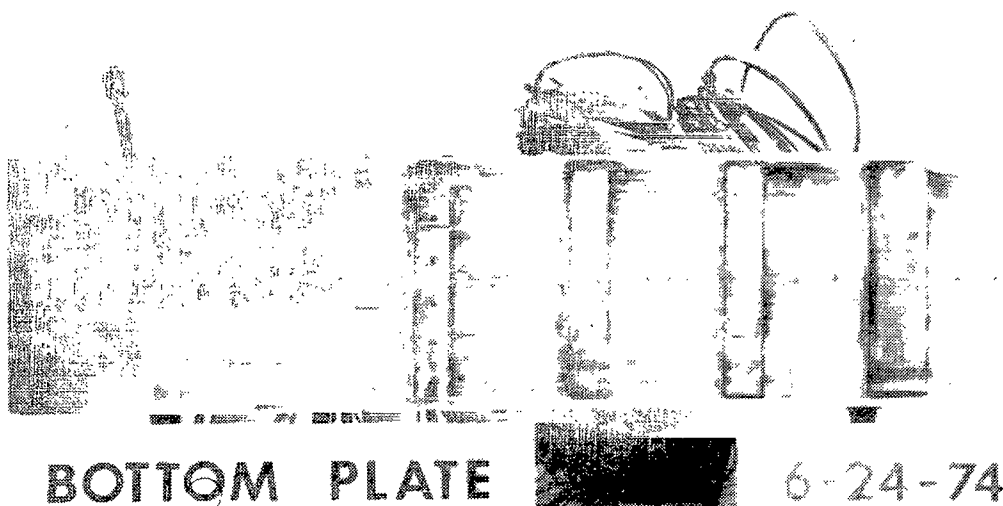
Figure 4. - Combustion duct photographs.
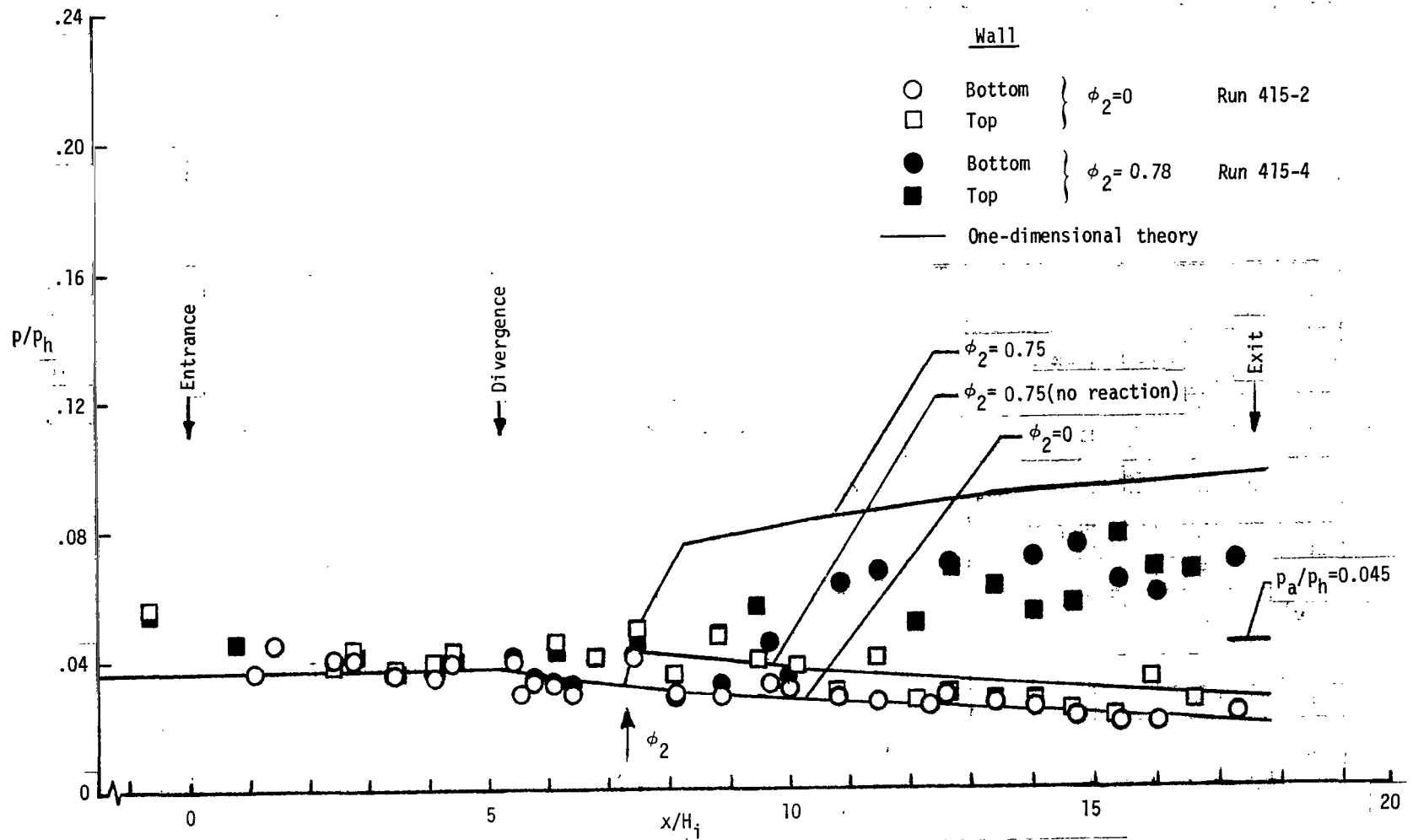
Figure 7.- Burner condition 1, wall pressure, second-stage injection.
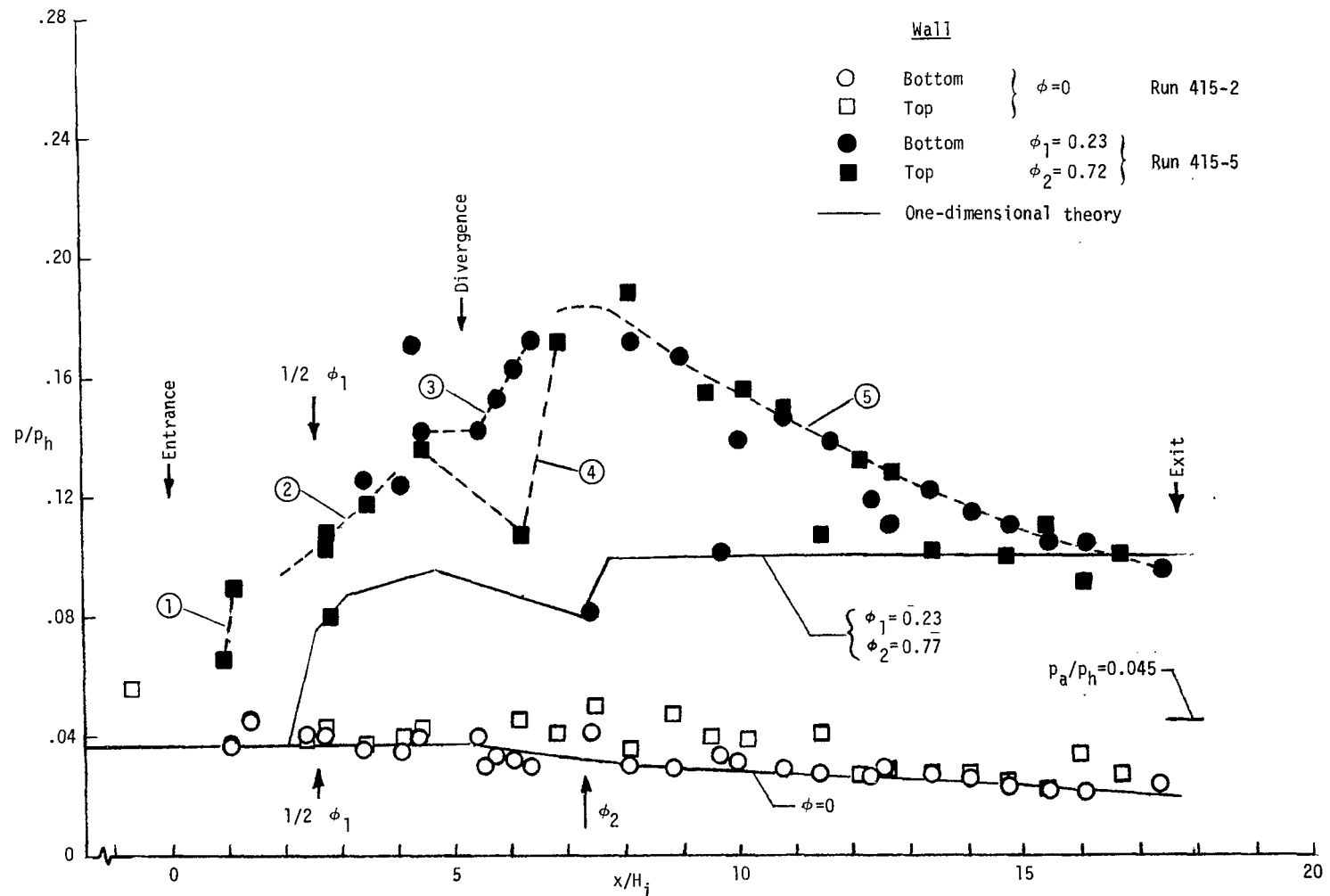
(a) Comparison of wall static pressure data with theory.

Figure 8.- Burner condition 1, wall pressure, two-stage injection.
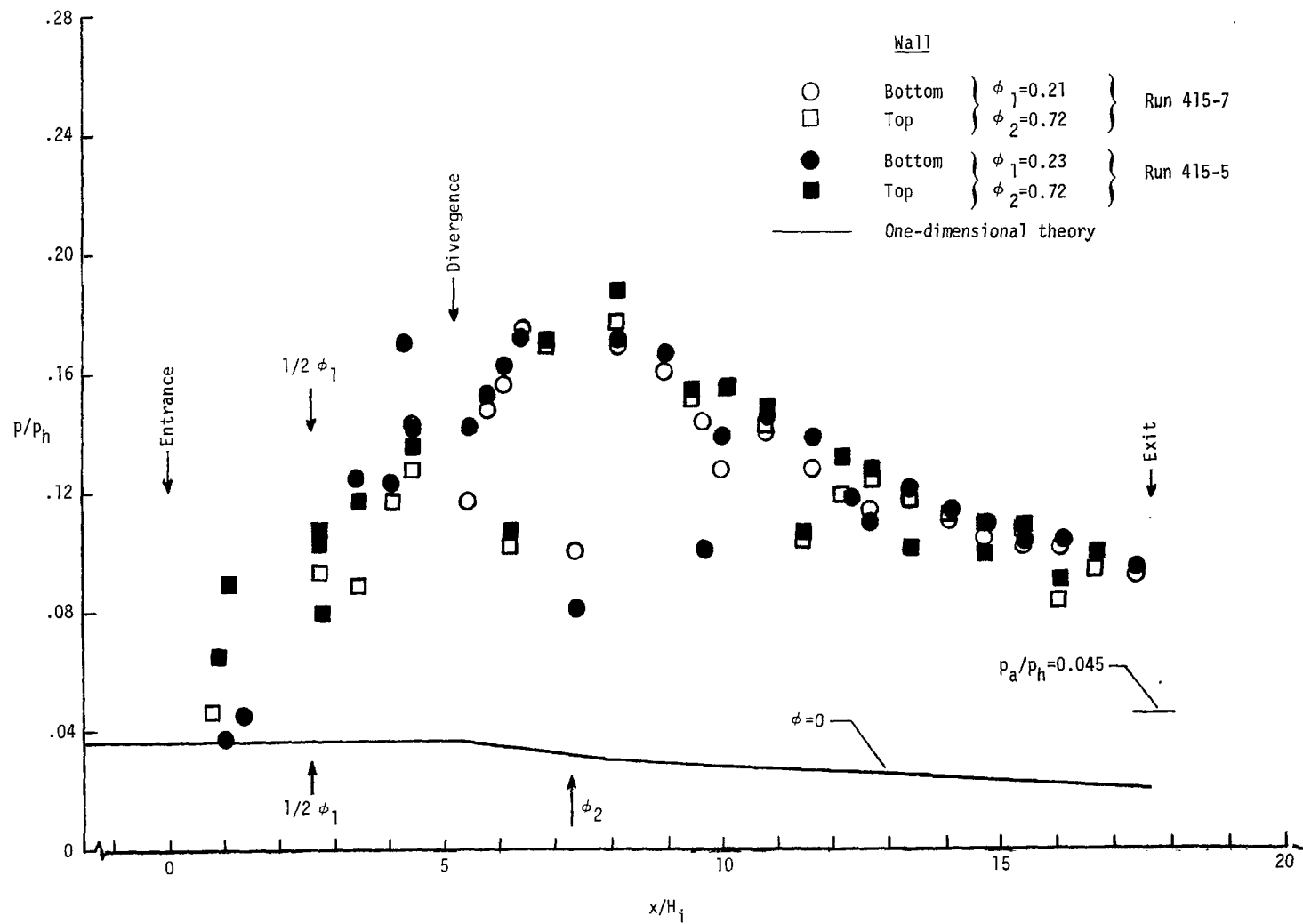
(b) Comparison of wall static pressure data repeatability.

Figure 8.- Concluded.
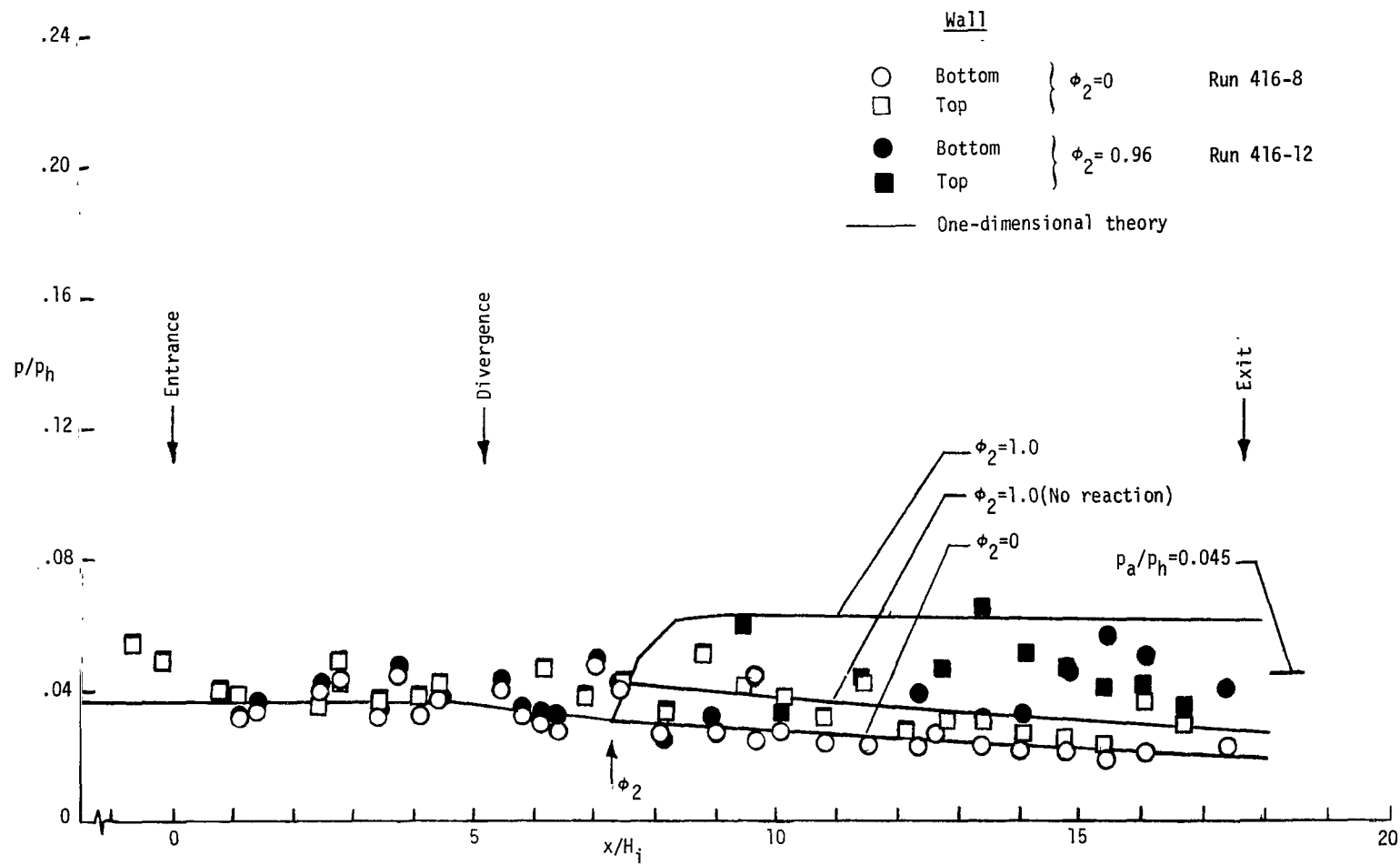
Figure 9.- Burner condition 2, wall pressure, second-stage injection.
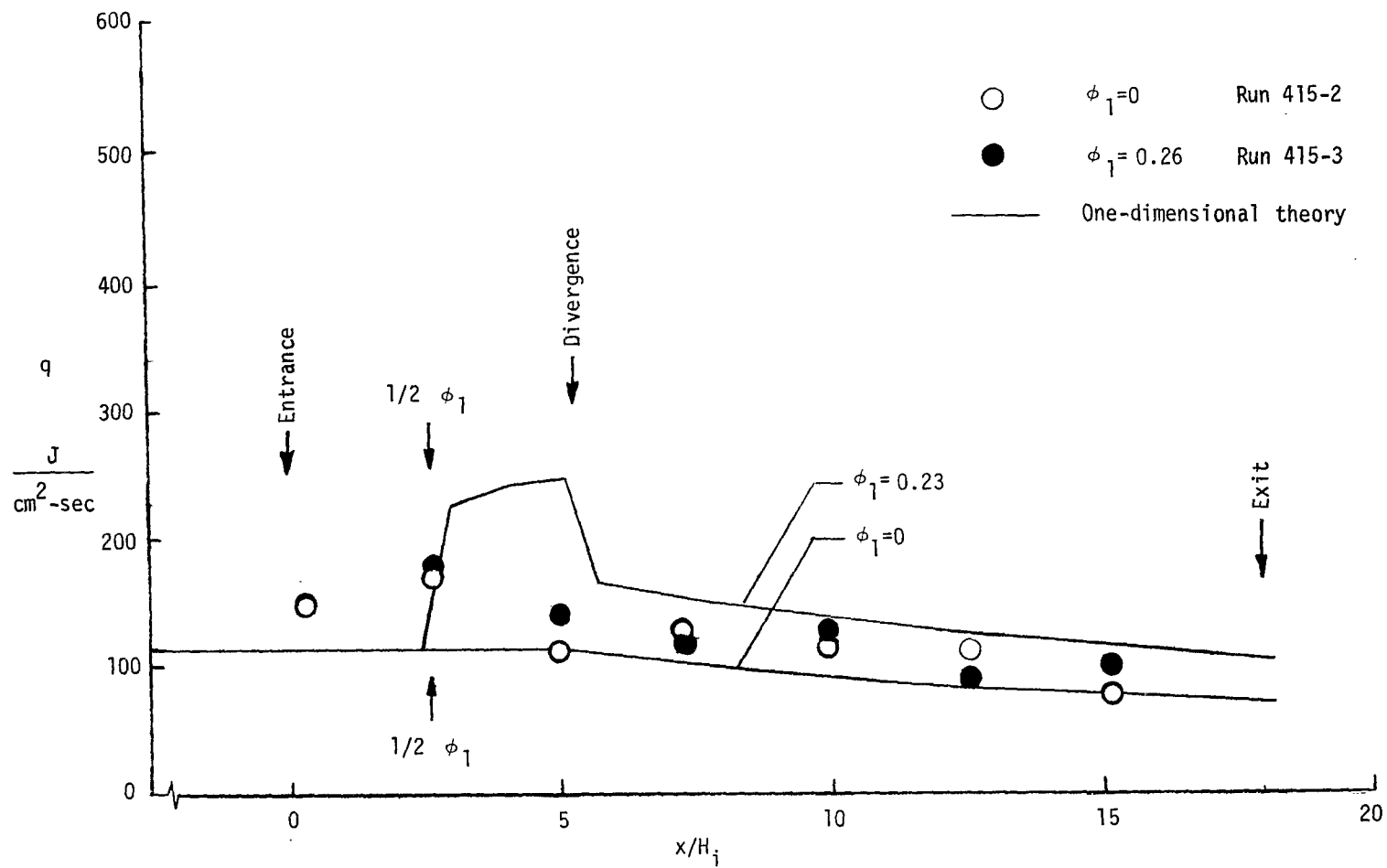
Figure 10.- Burner condition 1, bottom wall heat transfer, first-stage injection.
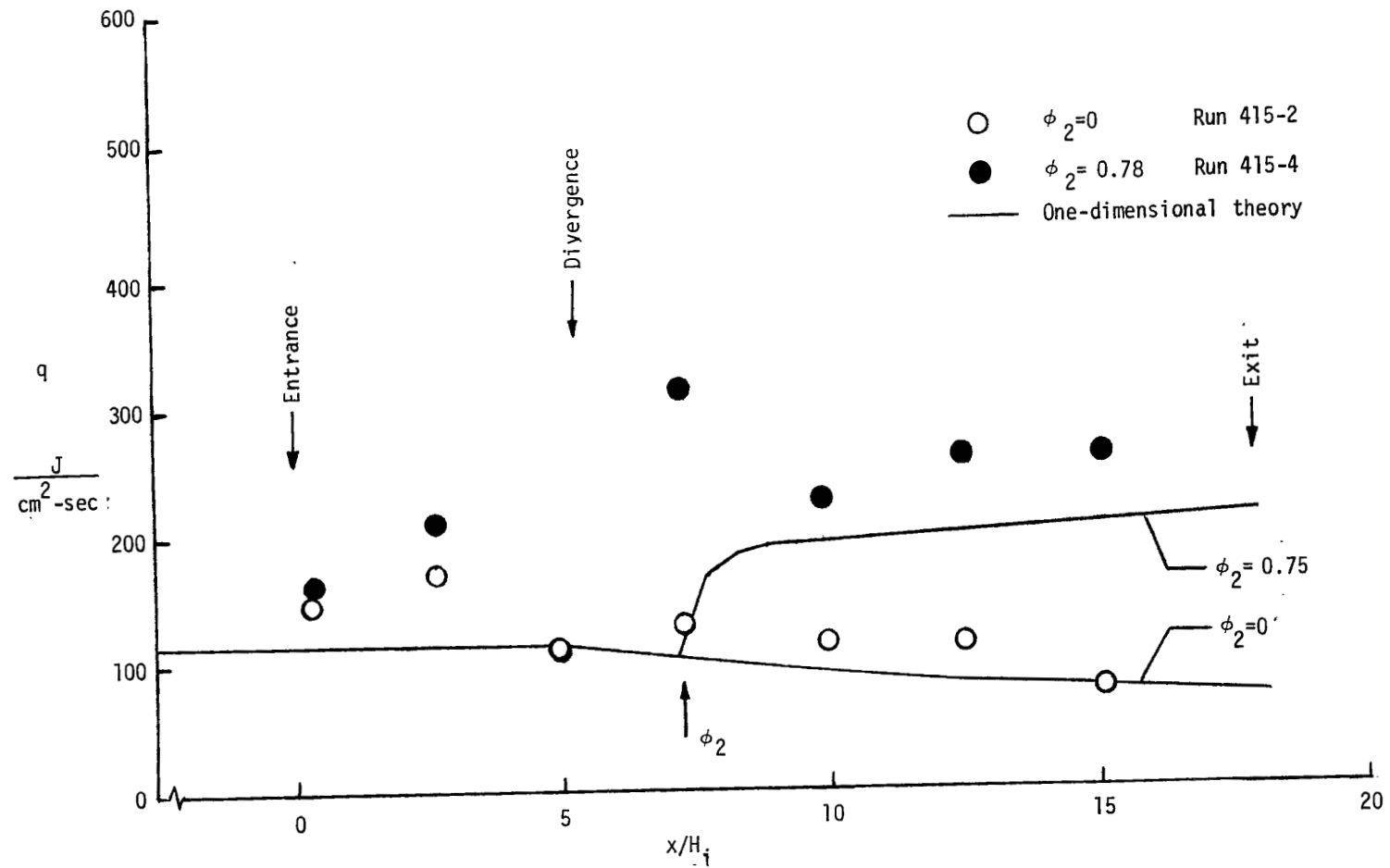
Figure 11.- Burner condition 1, bottom wall heat transfer, second-stage injection.
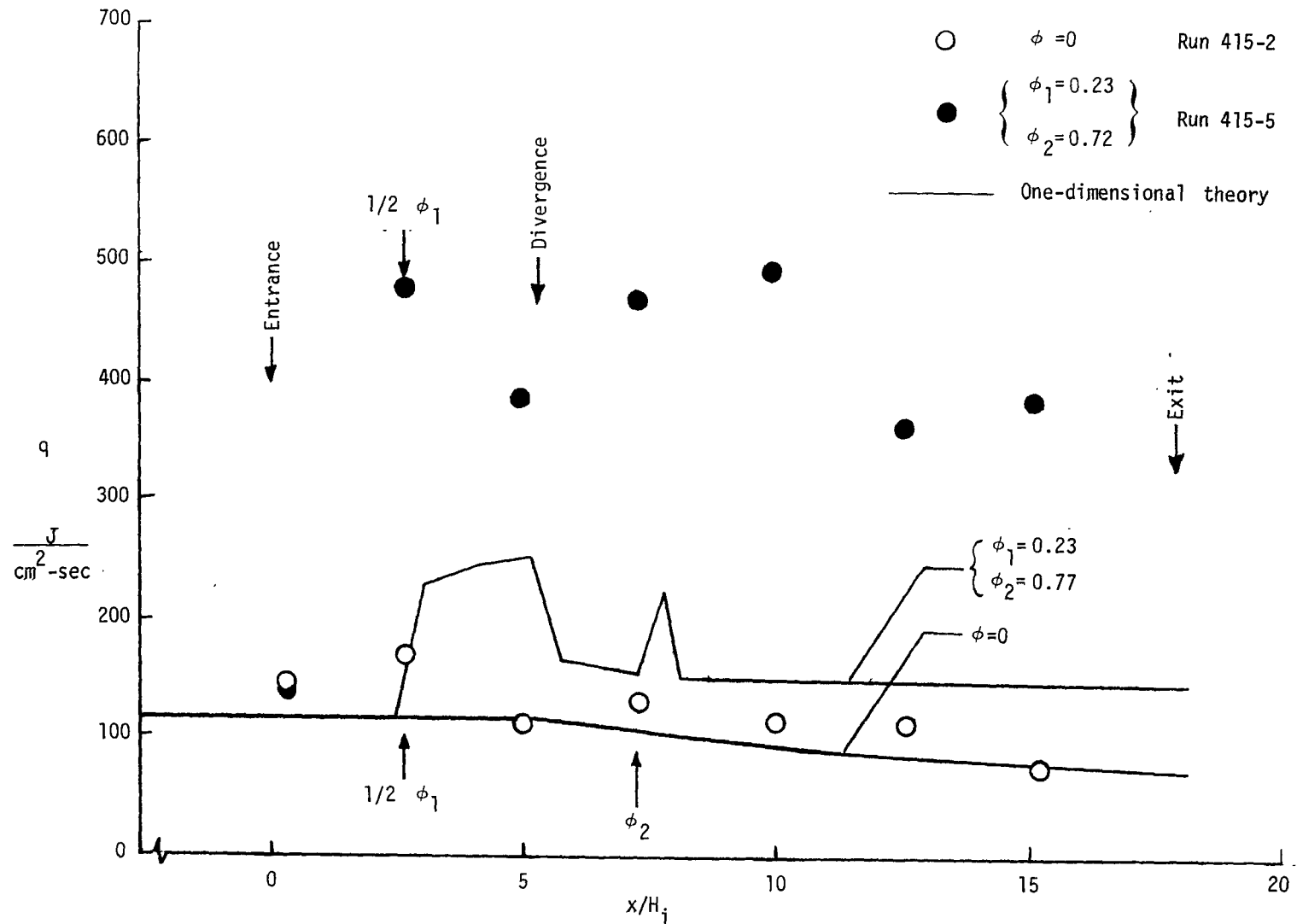
Figure 12.- Burner condition 1, bottom wall heat transfer, two-stage injection.
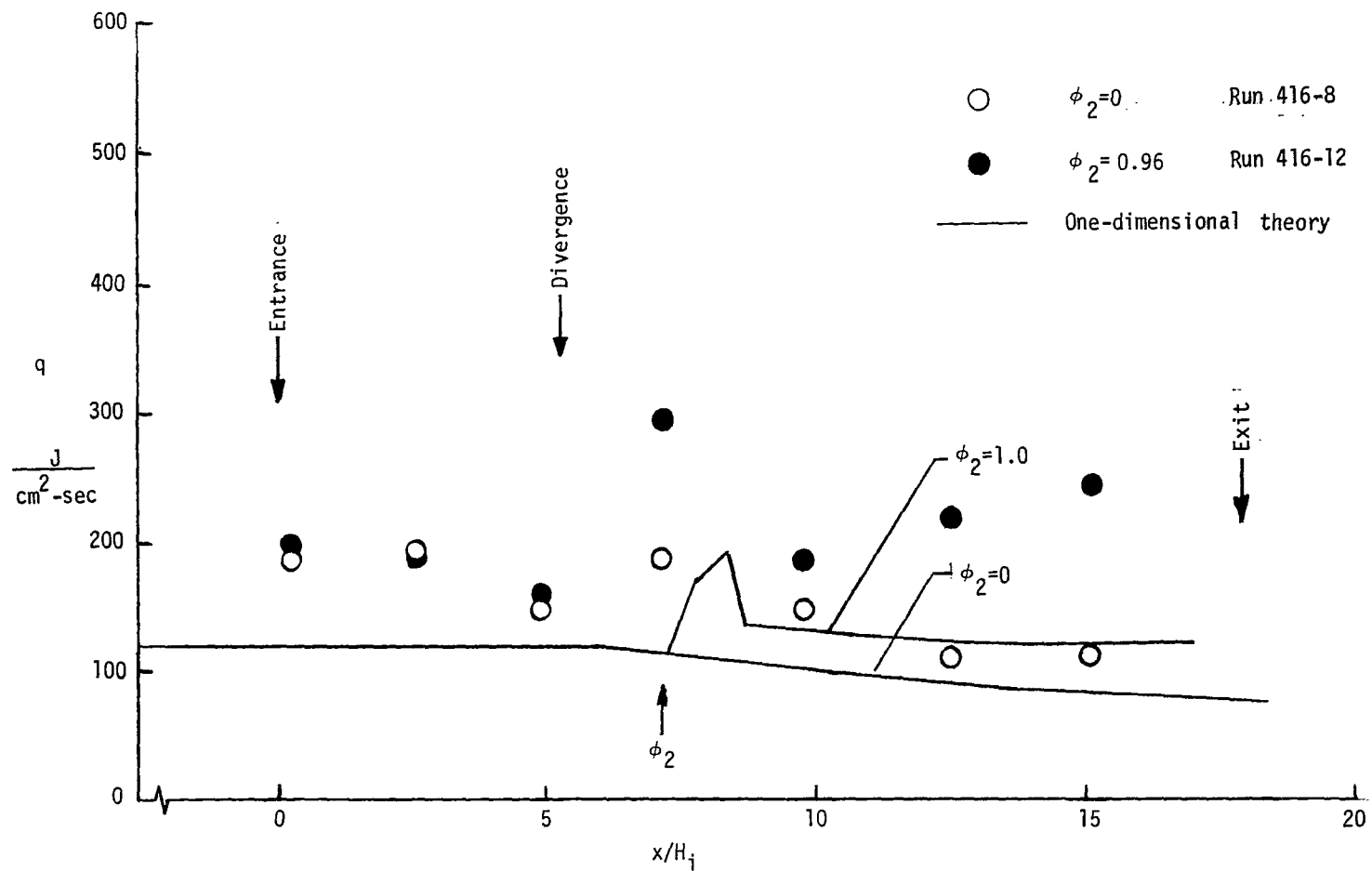
Figure 13.- Burner condition 2, bottom wall heat transfer, second-stage injection.
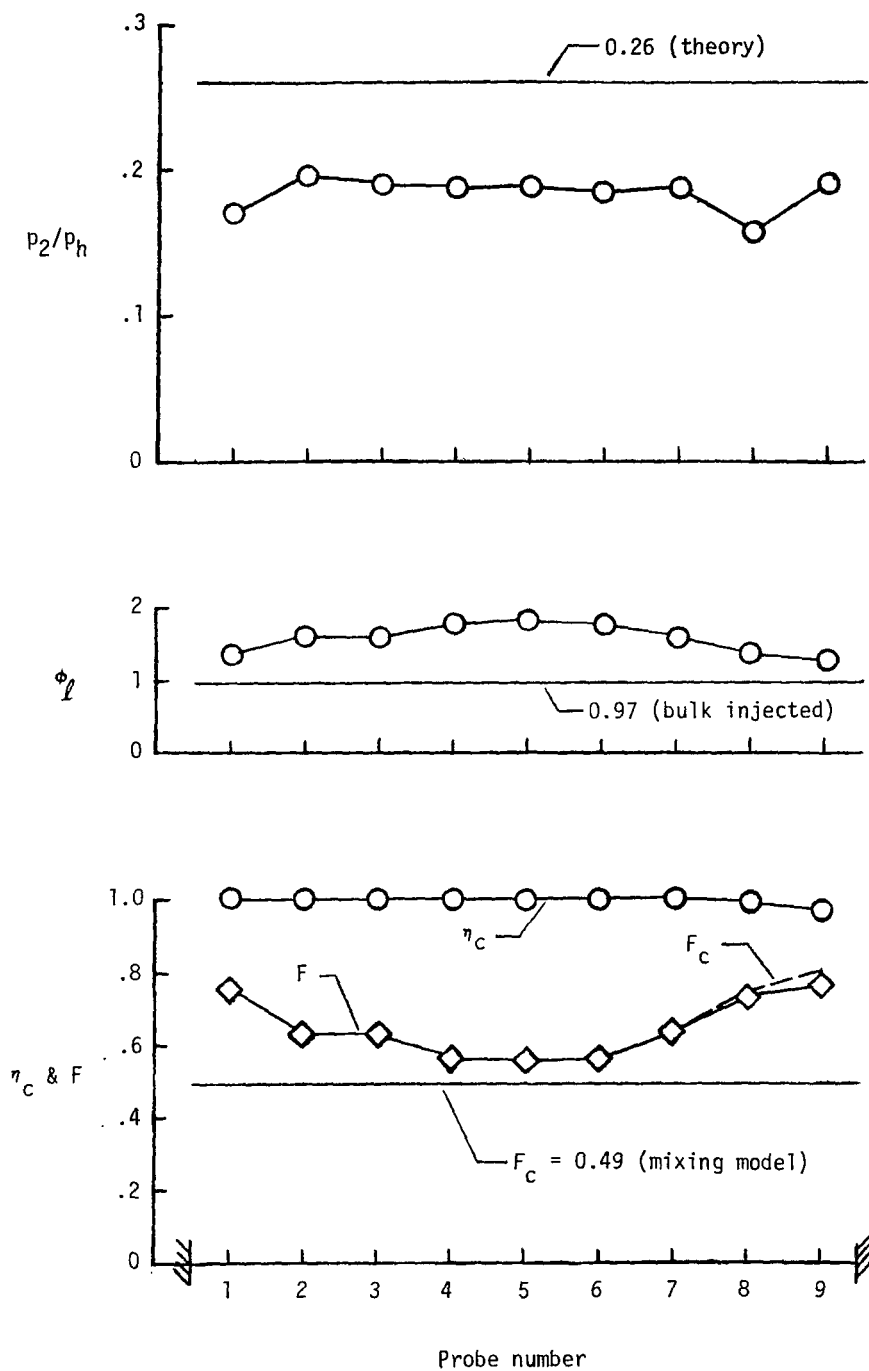
Figure 14.- Burner condition 1, combustion duct exit profiles, z/H_e = .213.

Run 415-8.
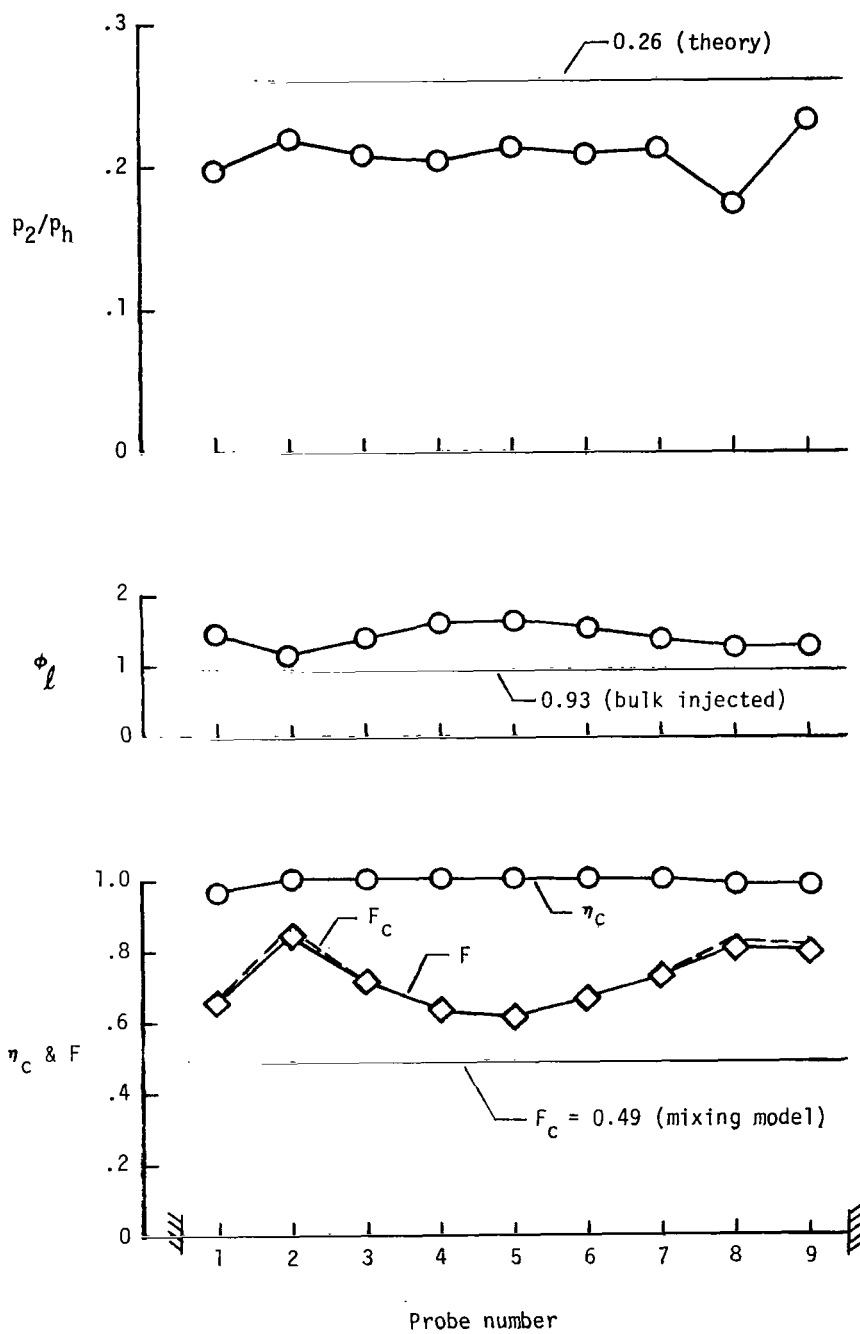
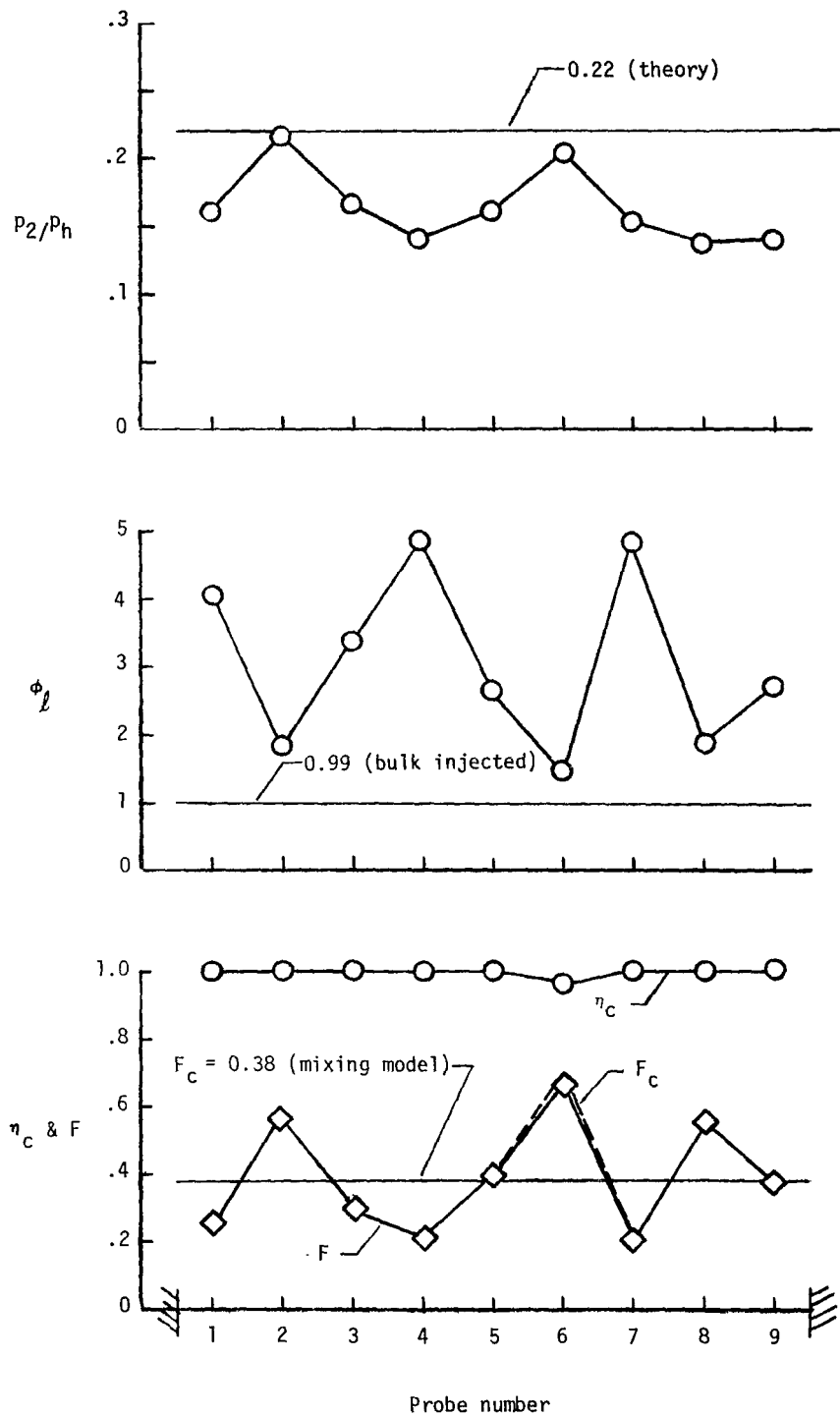Figure 15.- Burner condition 1, combustion duct exit profiles, z/H_e = .319. Run 415-7.
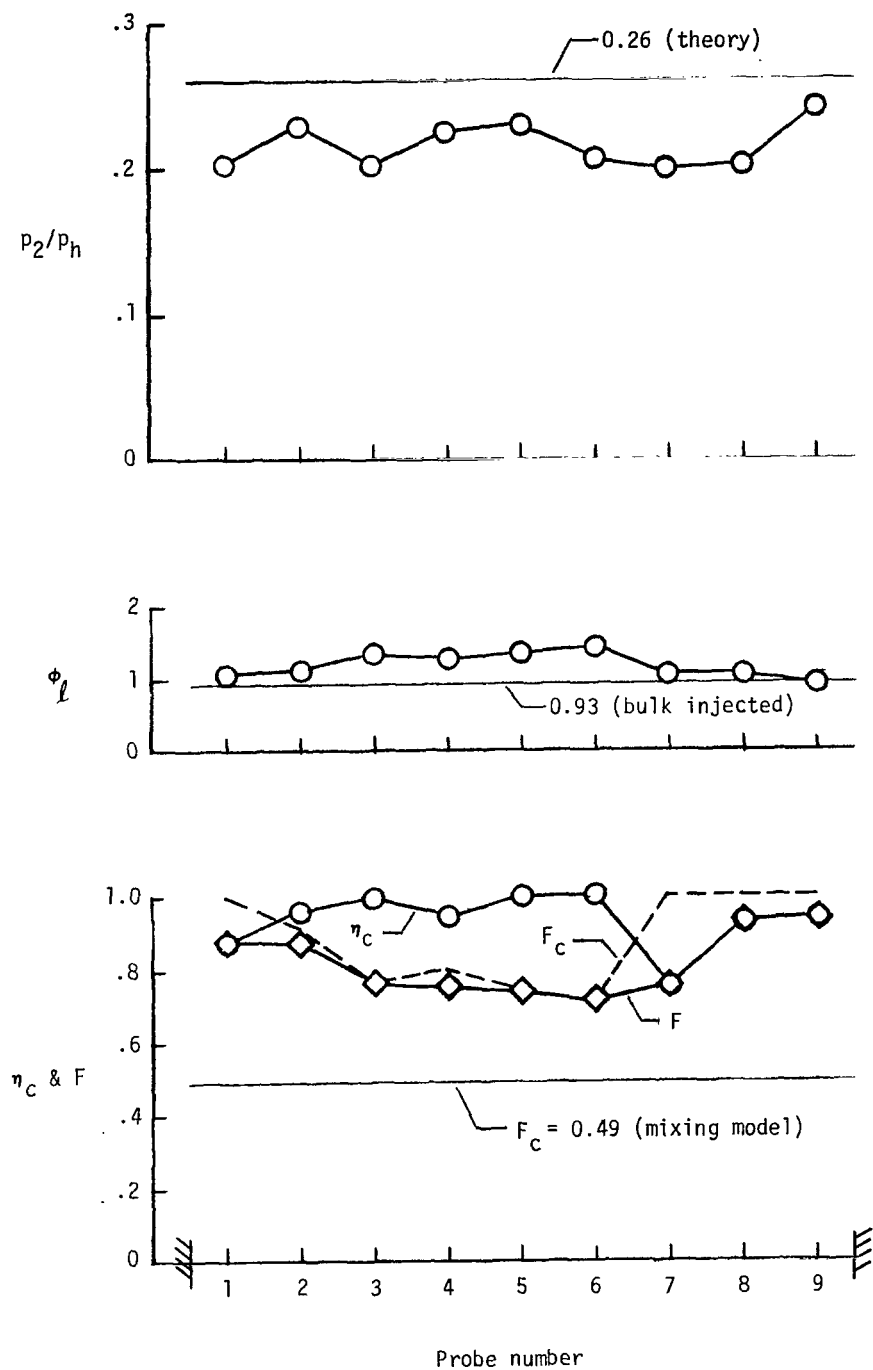
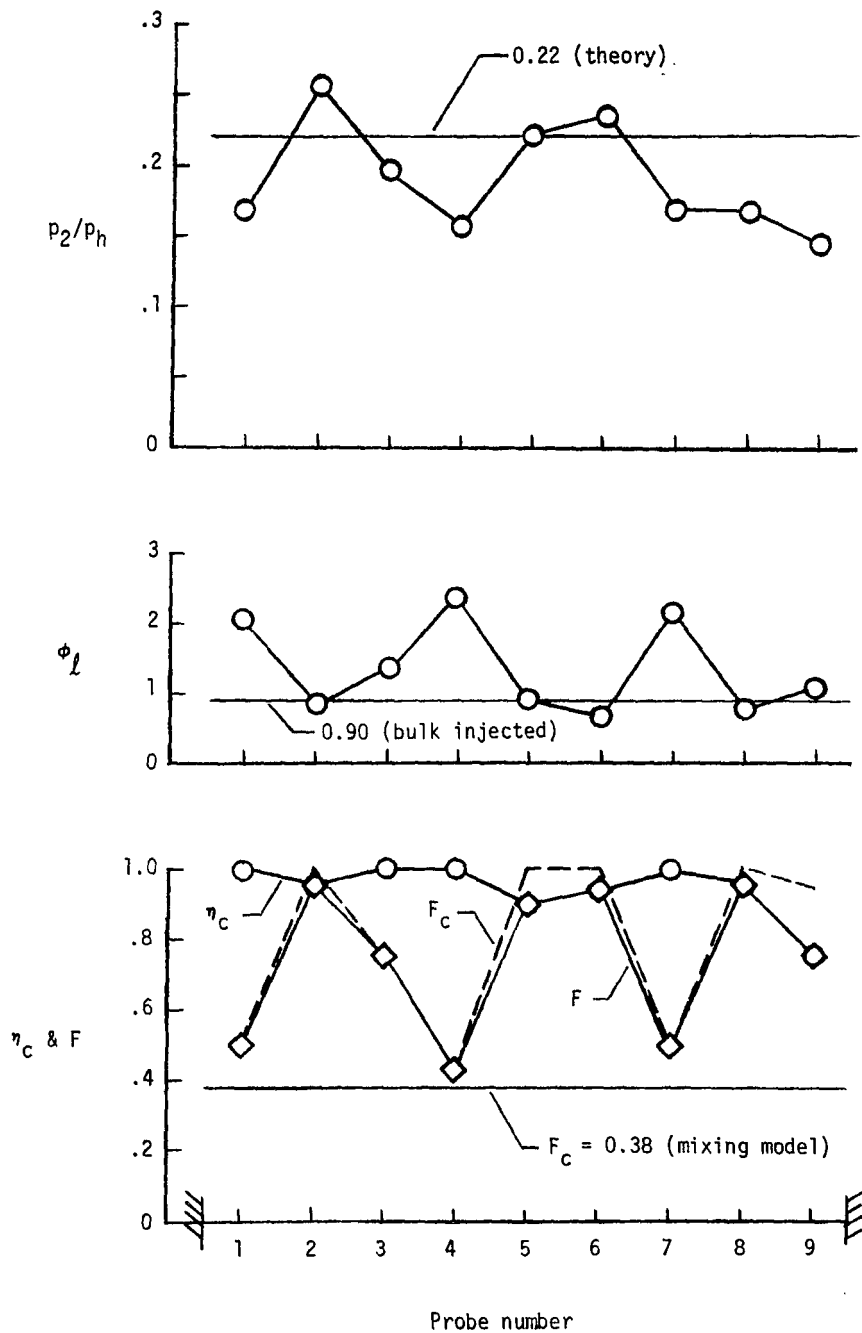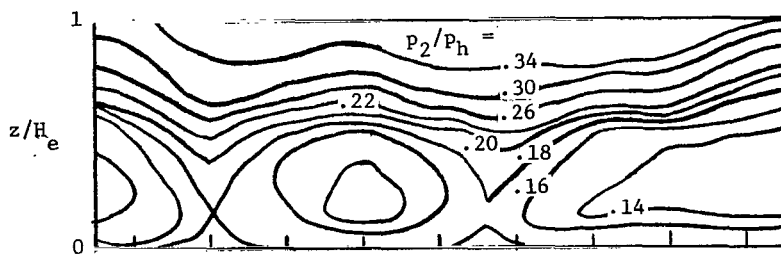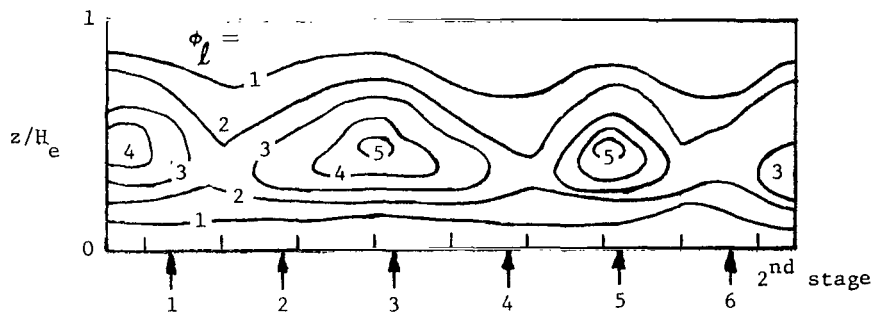Figure 16.- Burner condition 1, combustion duct exit profiles, z/H_e = .479. Run 415-6.
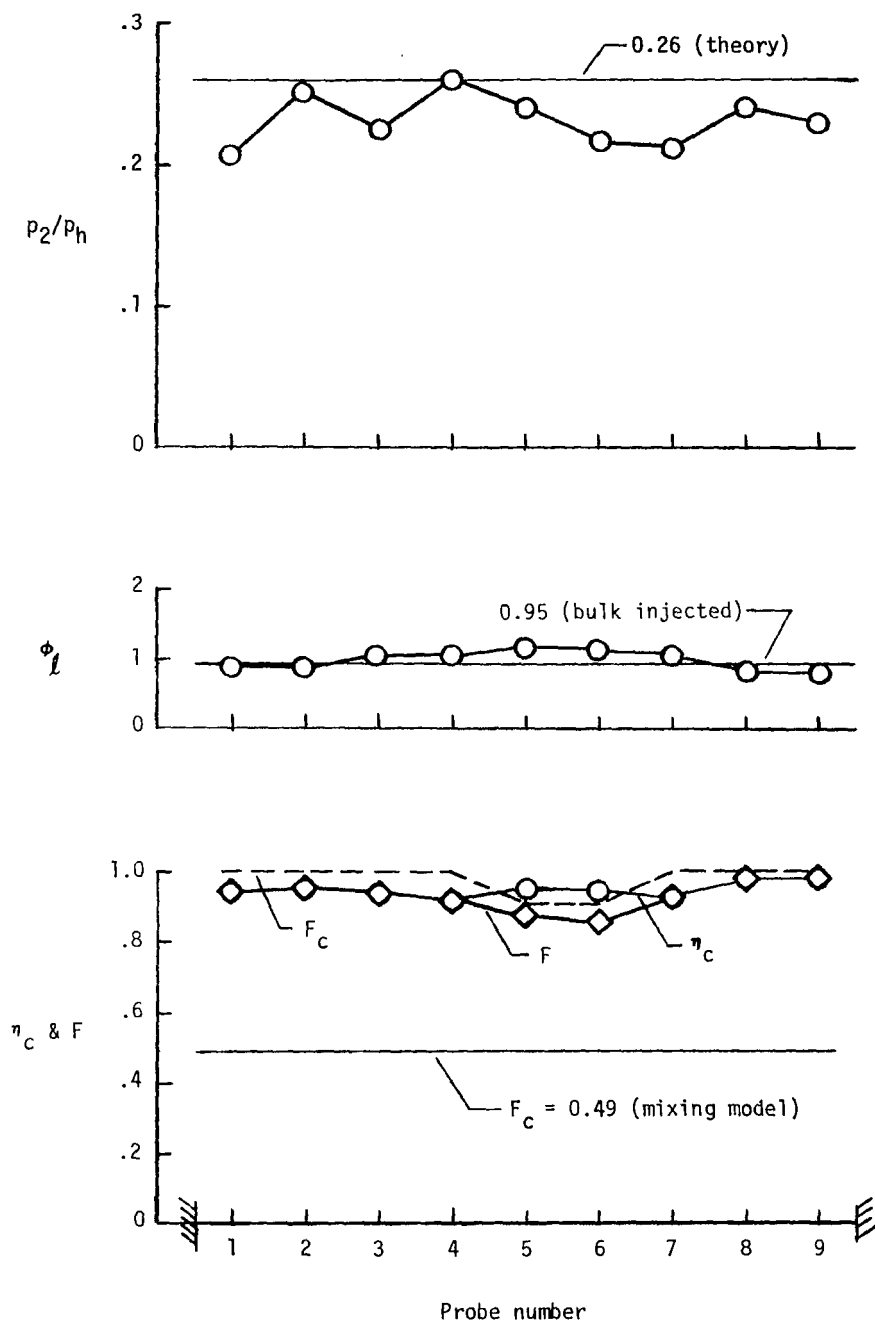
Figure 17.- Burner condition 1, combustion duct exit profiles, z/H_e = .649.
Run 415-9.
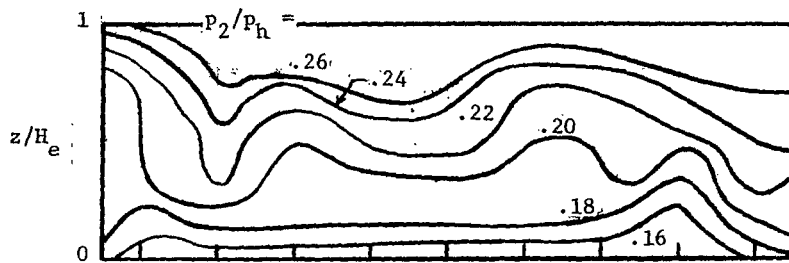
(a) Pitot pressure contours
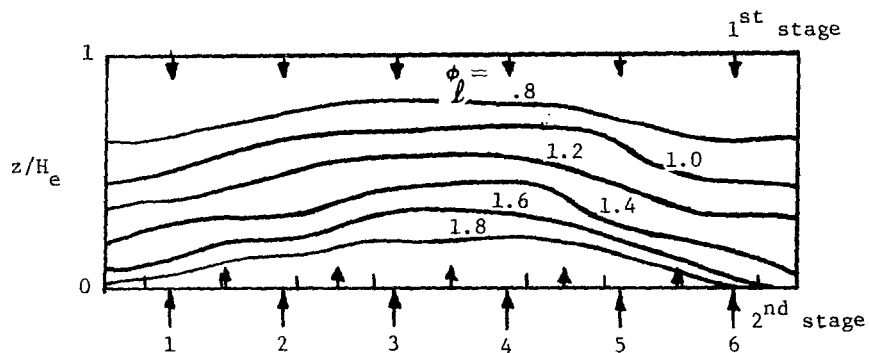
(b) Local equivalence ratio contours
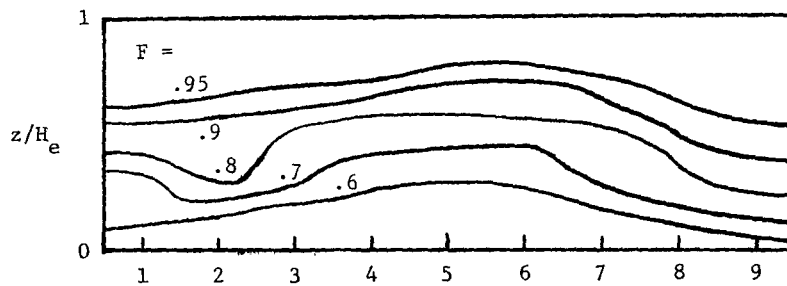
(c) Local fraction reacted contours

Figure 18.- Burner condition 1, combustion duct exit contours.
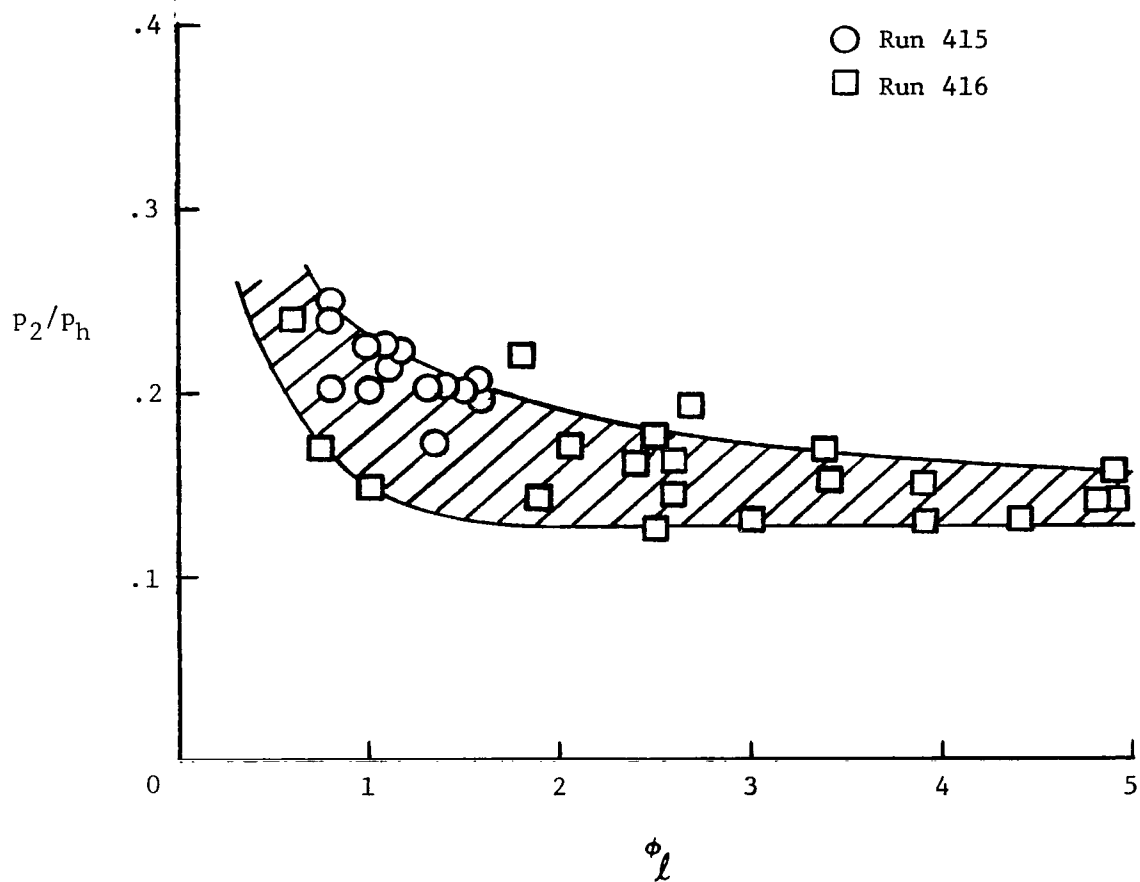
Figure 19.- Data correlation of pitot pressure and local equivalence ratio.
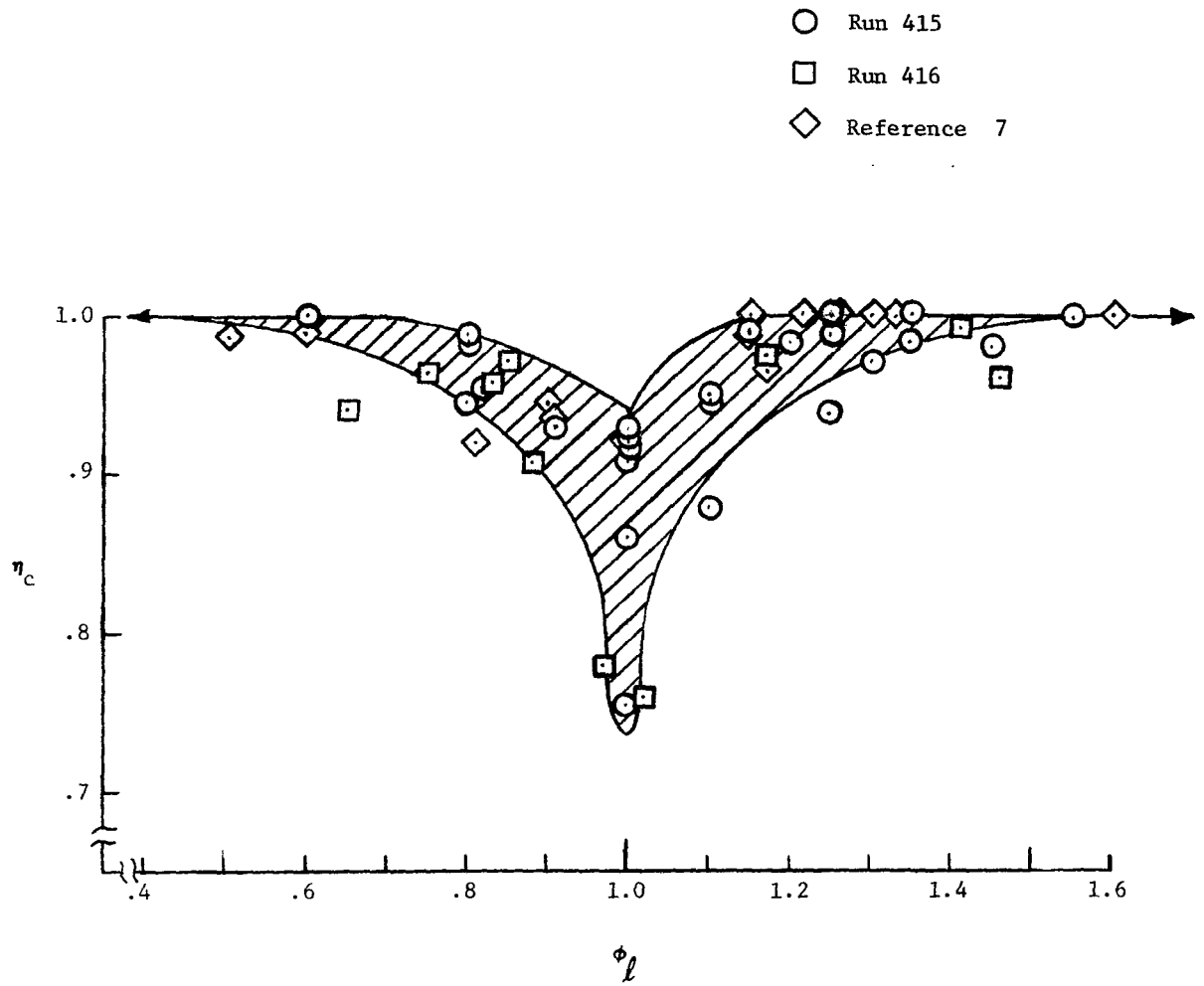
Figure 20.- Data correlation of combustion efficiency and local
equivalence ratio indicating the effects of chemical
kinetics and/or unmixedness.
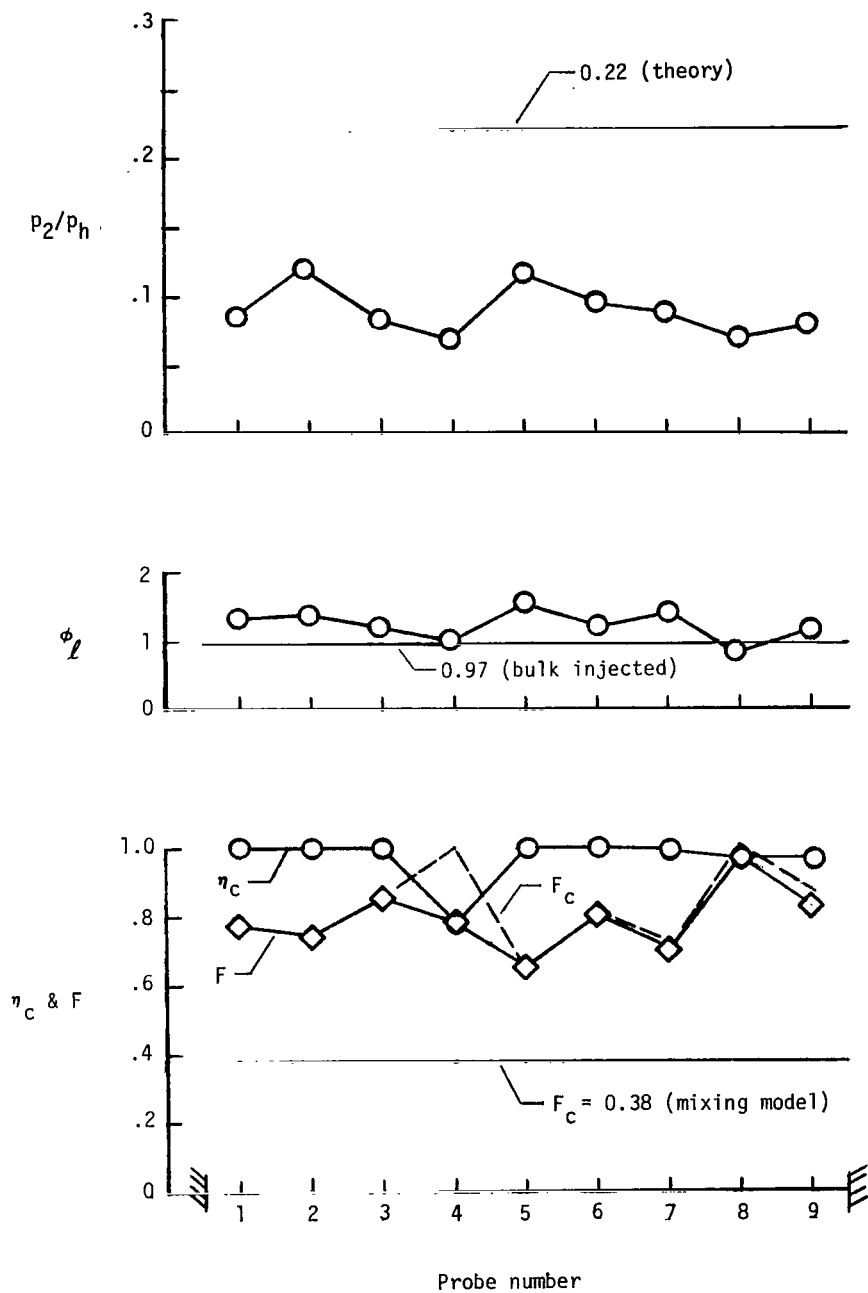
Figure 21.- Burner condition 2, combustion duct exit profiles, z/H_e = .160. Run 416-13.
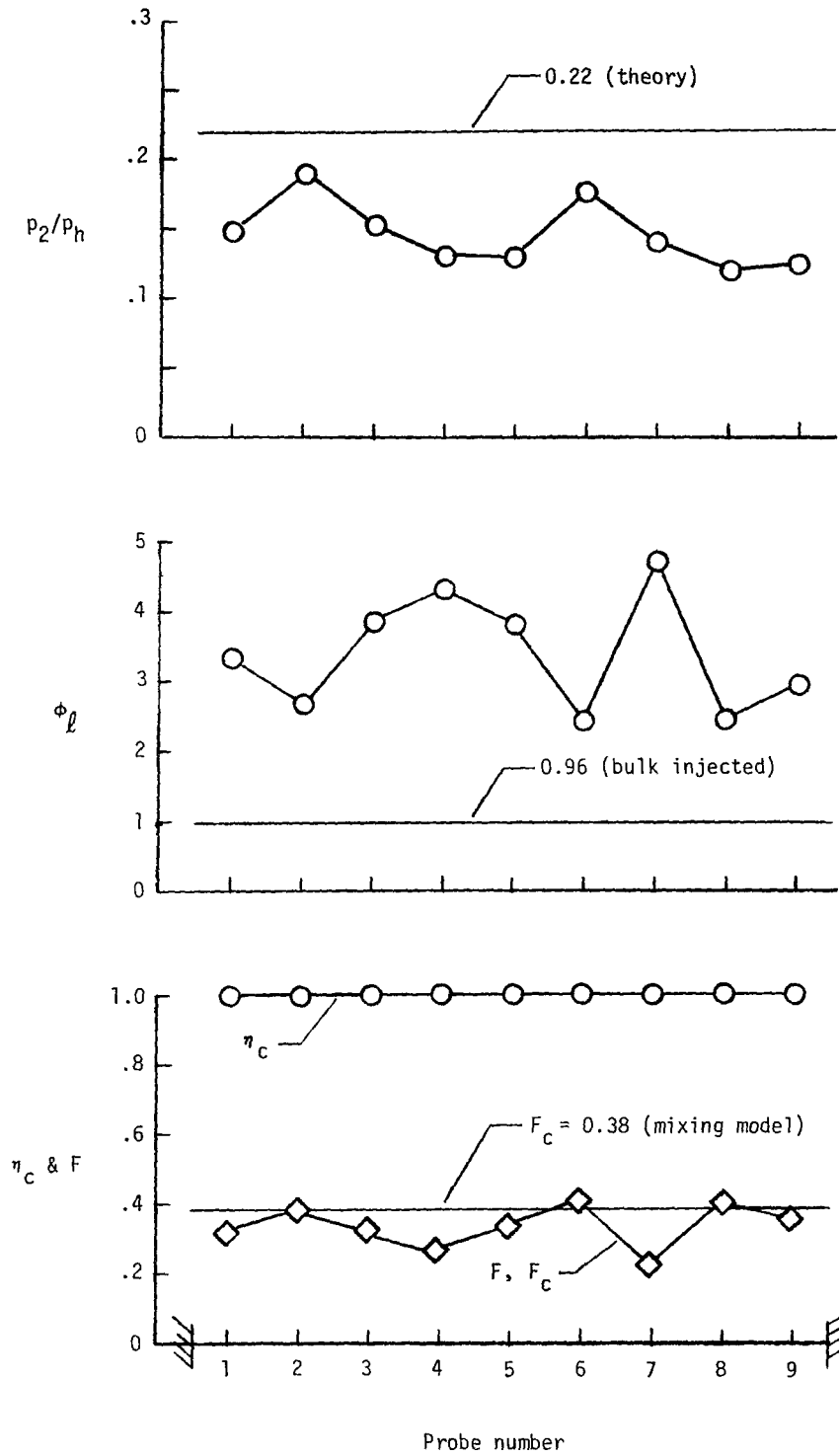
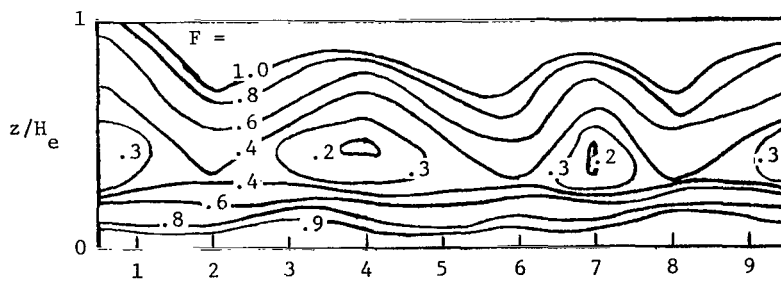Figure 22.- Burner condition 2, combustion duct exit profiles, $z/H_e = .319$.
Run 416-12.

Figure 23.- Burner condition 2, combustion duct exit profiles, z/H_e = .479.

Run 416-11.

Figure 24.- Burner condition 2, combustion duct exit profiles, z/H_e = .712.
Run 416-14.

(a) Pitot pressure contours

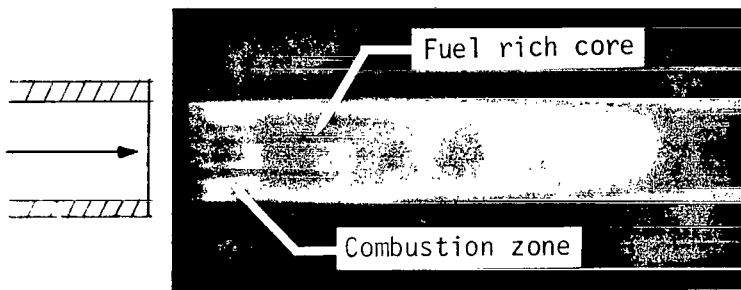(b) Local equivalence ratio contours

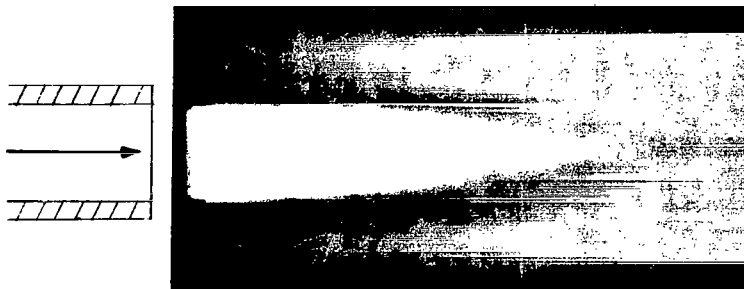Probe number

(c) Local fraction reacted contours

Figure 25.- Burner condition 2, combustion duct exit contours.
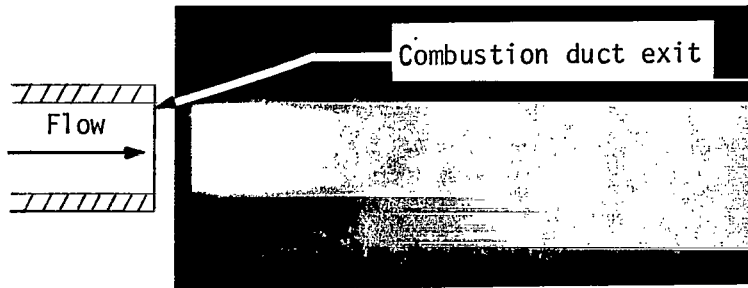
(a) First stage injection, Run 420-2-2

(b) Second stage injection, Run 420-3-3

(c) Two-stage injection, Run 419-12-1

Figure 26.- Top view of combustion duct exit flow.